

Metals and Dust in Intermediate-redshift Damped Ly- α Galaxies

Pushpa Khare¹

Dept. of Physics, Utkal University, Bhubaneswar, 751004, India

Varsha P. Kulkarni

Dept. of Physics and Astronomy, Univ. of South Carolina, Columbia, SC 29208

James T. Lauroesch

Dept. of Astronomy, Northwestern University, Evanston, IL, 60208

Donald G. York²

Dept. of Astronomy and Astrophysics, University of Chicago, Chicago, IL 60637

Arlin P. S. Crotts

Dept. of Astronomy, Columbia University, New York, NY, 10027

Osamu Nakamura

School of Physics and Astronomy, University of Nottingham, Nottingham, NG7 2RD, UK

ABSTRACT

We report spectroscopic observations with the Multiple Mirror Telescope for 11 damped Lyman-alpha absorbers (DLAs) or strong DLA candidates at $0.1 < z < 1.5$, including several absorbers discovered in the Sloan Digital Sky Survey. In particular, we have measured absorption lines of Zn II, Cr II, Ni II, Fe II, Mn II, Ti II, Ca II, and Si II. These measurements have doubled the sample of Zn and Cr measurements at $z < 1$. The average relative abundance patterns in these objects are very similar to those found for high-redshift DLAs reported in the literature. Our observations suggest that the dust content, as determined by $[\text{Cr}/\text{Zn}]$, does not show much change with redshift. We also examine the sample for correlation of $[\text{Cr}/\text{Zn}]$ with estimates of the quasar reddening. Our data suggest that the global mean metallicity of DLAs, as measured by the gas phase abundance of Zn, at best shows a weak evolution with redshift over the range $0.4 < z < 3.9$.

¹Also, Dept. of Physics and Astronomy, Univ. of South Carolina, Columbia, SC 29208

²Also, Enrico Fermi Institute, University of Chicago, Chicago, IL 60637.

Subject headings: quasars: absorption lines; galaxies: evolution; galaxies: abundances; cosmology: observations

1. Introduction

Observations of metallicity evolution in galaxies provide important constraints on the histories of gas consumption and star formation, because the global densities of gas, metals, and stars are closely coupled. Most cosmic chemical evolution models (e.g., Pei & Fall, 1995; Malaney & Chaboyer 1996; Pei, Fall, & Hauser 1999; Tissera et al. 2001; Somerville, Primack & Faber 2001) predict that the global mean interstellar metallicity in galaxies rises from nearly zero at high redshifts to nearly solar at $z = 0$. The present-day mass-weighted mean metallicity of local galaxies is also nearly solar (see, e.g., Kulkarni & Fall 2002). It is of great importance to determine whether the global mean metallicities of galaxies at intermediate and high redshifts agree with predictions of the cosmic chemical evolution models.

There is a long history of using damped Lyman-alpha absorbers (DLAs) to measure the gas phase abundances over the age of the Universe. It has been believed that DLAs constitute most of the neutral gas in the galaxies at high redshifts, enough to form all stars visible today (Wolfe et al. 1995). Furthermore, DLAs were also believed to provide an unbiased sample of normal galaxies as they are selected only through the presence of large amounts of neutral hydrogen. Recent data have raised questions regarding the validity of both these assumptions (Boisse et al. 1998; Rao & Turnshek, 2000; Kulkarni et al. 2001; Rao et al., 2003). Presence of dust and gravitational lensing can also affect the DLA statistics (Fall & Pei, 1993; Bartelman & Loeb, 1996). However, DLAs are still the primary source of information about the chemical abundances in galaxies over $> 90\%$ of the age of the Universe. A large number of elements have been observed in DLAs. In particular, Fe, Zn, Si, S and O have been used as probes of the metallicity in these systems. We prefer to use Zn to determine the total (gas + solid phase) metallicity in DLAs. This is because (i) Zn tracks Fe in most Galactic stars (e.g., Mishenina et al. 2002); (ii) it is relatively undepleted on interstellar dust grains; and (iii) the lines of the dominant ionization species Zn II are most often unsaturated. Abundances of depleted elements such as Cr, Fe or Ni relative to Zn probe the dust content of the absorbers (e.g., Pettini et al. 1997; Kulkarni, Fall, & Truran 1997).

DLAs are thus useful for testing predictions of cosmic chemical evolution models and are expected to show a rise in the global mean metallicity with decreasing redshift, if they indeed trace an unbiased sample of galaxies selected only by $N(\text{HI})$. However, it is unclear whether or not DLAs actually show such a trend. There has been great debate about this

issue, with most studies advocating no evolution in the global mean metallicity (Pettini et al. 1997, 1999; Prochaska & Wolfe 1999; Vladilo et al. 2000; Prochaska & Wolfe 2000; Savaglio 2001; Prochaska 2001; Prochaska & Wolfe 2002). In a reexamination of this issue for 57 Zn measurements in the range $0.4 < z < 3.4$, Kulkarni & Fall (2002) found that the slope of the metallicity-redshift relation is -0.26 ± 0.10 , consistent at $\approx 2\text{-}3\sigma$ level with model predictions (-0.25 to -0.61 , Pei & Fall, 1995; Malaney & Chaboyer, 1996; Somerville et al. 2001) as well as with no evolution. A similar slope (-0.25 ± 0.07) was also found more recently by Prochaska et al. (2003b).

One reason for the ambiguity in the metallicity-redshift relation is the large intrinsic scatter in the data. It is important to determine if the scatter apparent in the existing samples is cosmic scatter or is caused by errors of interpretation of the data. It is also important to observationally investigate whether DLA samples are being affected by dust obscuration. We address both these issues in this paper. The other reason for the lack of accurate metallicity-redshift relation is the small number of measurements available, especially at $z < 1.5$. Most previous DLA Zn studies have focused on $z > 1.5$ because the Zn II $\lambda\lambda$ 2026, 2062 lines lie in the ultraviolet (UV) for $z < 0.6$, and likewise for Lyman- α for $z < 1.6$. For $0.6 < z < 1.3$, the Zn II lines can be accessed with ground-based telescopes, but lie in blue wavelengths where many spectrographs have lower sensitivity. It is very important to obtain more data at $z < 1.5$, because this regime spans $\sim 70\%$ of the age of the Universe (for $\Omega_m = 0.3$, $\Omega_\Lambda = 0.7$; Ω_m and Ω_Λ being the mean comoving matter density and vacuum energy density of the universe, respectively, in units of the critical energy density of the universe). The low- z data provide great leverage on the slope of the metallicity-redshift relation, and can clarify the relation of DLAs to present-day galaxies. A lack of metallicity evolution would contradict the high global star formation rate at $1 < z < 1.5$ inferred from the galaxy surveys such as the Canada France redshift survey, Hubble Deep Field, as well as the Sloan Digital Sky Survey (SDSS) (e.g. Lilly et al. 1996; Madau et al. 1996; Glazebrook et al. 2003). It would imply that either DLAs systematically trace only metal-poor dwarf or low surface brightness galaxies, or that the more metal-rich and dustier DLAs obscure their background quasars. Clearly, it is necessary to pin down the shape of the metallicity evolution in a more definitive way.

As a first step toward improving the statistics of the metallicity-redshift relation at intermediate redshifts, we have recently started a survey of element abundances for DLAs or strong DLA candidates (hereafter, CDLAs) at $z < 1.5$ discovered with the SDSS or the Hubble Space Telescope (HST). Here we report the results of this survey for a sample of 11 DLAs with $0.09 < z < 1.5$. Our observations and data reduction are described in section 2. Section 3 explains the determination of column densities. Notes on individual objects are presented in section 4. Section 5 describes our results. Finally, a discussion of our results

and implications for the redshift evolution of dust content and metallicity are presented in Section 6.

2. Observations

Our sample consists of quasar absorbers at $0.09 < z < 1.5$, for which either a damped Lyman- α line is observed in HST spectra, or a strong DLA is expected on the basis of Mg II or Fe II lines (Rao & Turnshek, 2000) available in the SDSS Early Data Release (EDR) spectra (Schneider et al. 2002; York et al. 2005a). In particular, we have chosen systems that have $W_{\text{MgII}2796}^{\text{rest}} > 1.0 \text{ \AA}$ and some other indicator of high $N(\text{HI})$ (Fe I, C I, Mg I, Mn II, Ni II, Ca II, Cr II, Zn II or Si II $\lambda 1808$). For six of these SDSS systems $W_{\text{FeII}2344}^{\text{rest}} > 0.79 \text{ \AA}$. In the case of the $z_{\text{abs}} = 1.0311$ system in SDSS1727+5302, $W_{\text{FeII}2344}^{\text{rest}} = 0.56 \text{ \AA}$, but this quasar was observed because of the other system at $z_{\text{abs}} = 0.9449$ in its spectrum. Objects which met these selection criteria and which could be observed on our assigned nights constitute our target list, given in Table 1. The table lists the name of the QSO; plate number, fiber no. and Mean Julian Date (MJD) of the Sloan Digital Sky Survey (SDSS) observation used to select the targets; the emission line redshift of the QSO; the SDSS g magnitude (Fukugita et al. 1996); the redshift for the DLA targeted in the observation; the grating used for the Multiple Mirror Telescope (MMT) observations; the FWHM achieved for the calibration lamp emission lines; the exposure time; and the signal-to-noise ratio (S/N) achieved per pixel. The overview of the SDSS project is given by York et al. (2000) and the data products are described by Stoughton et. al (2002). The camera used for the imaging observations are described by Gunn et al. (1998). The use of colors derived from the camera to select QSOs for spectroscopy is described by Richards et al. (2002). The data are rereduced and republished as new objects are observed. Data Release 1 (Abazajian et al. 2003) and Data Release 2 (Strauss et al. 2004) give modifications to the EDR data formats and products. The spectra used in this paper are on the SDSS project web site (<http://skyserver2.fnal.org>). The measurements used for selecting our targets, as modified by rereductions for inclusion in the tables below, are from York et al. (2005a).

Previous data on these DLAs are listed in Table 2. Following a four digit designation (see Table 1) of the QSO and a two digit version of the absorber redshift from later tables are given the rest frame equivalent widths for the strong lines of Fe II in multiplets UV1 and UV3 and Mg II (UV1), as well as those of some weaker lines we used to select the systems for observation: Mn II (UV 1); Mg I $\lambda 2853$ (UV 1); and Ca II multiplet 1. Where available, the 1 sigma rest equivalent width errors are listed just below the equivalent widths (even rows 4 thru 18). The sources are listed in the footnotes.

Our new observations were obtained at the 6.5 m MMT, during October 10-12, 2002 and March 23-25, 2003. Approximately 1.8 nights were lost to bad weather. The blue channel spectrograph was used with a 832 l/mm grating in the second order and a 1200 l/mm grating in the first order. A CuSO_4 order sorting filter was used to block first order red light when using the 832 l/mm grating in second order. The total wavelength range covered for 832 l/mm grating was from 3280 Å to 4420 Å and that for 1200 l/mm grating was 3920 Å to 5420 Å. Each grating was used with somewhat different central wavelength settings for different DLAs, depending on its redshift. The dispersions were 0.36 Å per pixel and 0.50 Å per pixel respectively, for the 832 and 1200 l/mm gratings. A 1.0'' wide slit was used. In order to achieve the required S/N while avoiding cosmic rays, we took several exposures of each object of durations 1800 s or 2700 s depending on their magnitudes. Each exposure was preceded and followed by He+Ne+Ar lamp exposures as well as quartz lamp flat field exposures to get accurate wavelength calibration and flat fielding. Biases, additional quartz flats, and spectra of bright stars were taken in the beginning and end of each night.

The data were reduced using the standard spectrographic reduction packages of IRAF¹. Instrumental resolution was obtained from Gaussian fits to the lamp lines near the wavelengths of all lines to be analyzed in the object spectra. It varies from 1.04 Å to 1.54 Å over most of the wavelength range. The continuum-fitted spectra with line identifications for the confirmed DLAs and CDLAs are given in Figs. 1-8. All lines more significant than 3σ in the DLAs were identified and measured for equivalent widths using the `splot` task in IRAF. The absorption systems found are given letter designations A, B,..., which are listed beside the redshifts, in increasing order, across the top of the plots. The figures, in some cases, also include tick marks at the expected positions of lines discussed later on in the text, which have not been detected.

Table 3 lists the atomic data (species, vacuum laboratory wavelength, oscillator strength and reference for the data source) used for the identification of lines and for the reductions.

Table 4 lists the rest-frame equivalent widths, with 1σ errors, of the various heavy element lines measured for each system. For lines which are blended with stronger lines of other systems, we give the equivalent width of the blend as an upper limit. For weaker (below the 3σ detection limit) lines of those species for which the stronger lines have been observed, we give the 3σ upper limit on the equivalent width, obtained assuming the line to be three pixel wide. The table lists the QSO by the first four digits of its designation in

¹IRAF is distributed by the National Optical Astronomy Observatories, which are operated by the Association of Universities for Research in Astronomy, Inc., under cooperative agreement with the National Science Foundation.

Table 1, and the letter designation of the system; the absorption line redshift, determined from the average redshifts of the unblended lines of the system detected at the 4σ level; the species; the rest wavelength; and the difference between the redshift determined for that line and the redshift in column 2. This Δz is given in units of 10^{-5} , so, for instance an entry of 5 at z of 1 corresponds to 7.5 km s^{-1} or 0.1 \AA at 4000 \AA , about $1/4$ of a pixel width (832 l/mm grating, 2^{nd} order) or $1/5$ of a pixel width (1200 l/mm grating 1^{st} order).

3. Determination of column densities

The reasonably high values of S/N for our data made it possible to perform profile fitting analysis using the package FITS6P (Welty et al., 1999, 2001).

The lines of Zn II and Cr II are often strong, stronger than those detected in some other studies. For instance, our average rest frame equivalent widths of the blend of Zn II and Mg I lines at 2026 \AA and of Cr II line at 2056 \AA are 182 m\AA and 152 m\AA respectively, while those of Pettini et al. (1994) are 92 m\AA for both lines. This may be partly due to the fact that in order to ensure the DLA nature of the absorbers, we have chosen systems from the SDSS spectra that have strong Mg II and Fe II lines and some other indicator of high $N(\text{HI})$ (C I, Mg I, Si II $\lambda 1808$, Mn II, Ni II, Ca II, Cr II, or Zn II). We thus could have chosen DLAs at the high column density end (which after all dominate the N_{HI} -weighted global mean metallicity). However, in principle, it is also possible that, due to chemical evolution, the abundances at lower redshift are higher than the abundances at the redshifts (> 2) observed, e.g., by Pettini et al. (1994), which may be responsible for the higher line strengths measured by us.

At the resolution of $75\text{-}95 \text{ km s}^{-1}$, it is not possible for us to resolve the Mg I $\lambda 2026$ line from the Zn II $\lambda 2026$ line, and the Cr II $\lambda 2062$ line from the Zn II $\lambda 2062$ line. Therefore, in determining the column densities of Zn II and Cr II, we have used information about other lines of Mg I, wherever necessary, and of Cr II. For Mg I, we have determined the column density from the equivalent width of the Mg I $\lambda 2853$ line observed by the SDSS or by other observers as listed in Table 2, using the b value obtained from the profile fit as described below. It is possible that the Mg I column density as obtained from the $\lambda 2853$ line may be affected by saturation effects, however, no other line of Mg I is detected. We have tried to estimate the effect of the uncertainty in the Mg I column density on the column densities of Zn II as described below. For Cr II $\lambda 2062$, we have used the Cr II $\lambda\lambda 2056, 2066$ lines.

The general method followed for the analysis of the Zn II, Cr II, Mg I lines between 2025 \AA and 2070 \AA was as follows. We assumed the central velocity, v , and the effective

velocity dispersion, b , of these lines to be same.

1. The lines of Cr II $\lambda\lambda$ 2056, 2066 were fitted first.
2. The above two lines plus Zn II λ 2062 and Cr II λ 2062 were fitted simultaneously, using as starting values the results of step 1. The common central velocity, the common effective b values and the two column densities were all varied to get the best fit.
3. Using the results for the four lines of step 2, the lines were refit, including Zn II λ 2026 and Mg I λ 2026. In some cases, where we could derive the column density of Mg I, we compared it with the value derived from the SDSS equivalent width of λ 2853, to check for consistency. In others, the data for λ 2853 along with the b value obtained after step 1 and 2, were used to obtain values or limits that were used for the Mg I λ line and the other five lines were allowed to vary.
4. Sometimes, when it was not possible to fit the Cr II λ 2056 line because of noise or a blend, and so it was not possible to determine the b value, we took the b value for the Zn II, Cr II and Mg I lines to be the same as that for Si II or for Fe II. In principle the effective b value for the Fe II or Si II lines could be larger than that for the Zn II and Cr II lines, if the latter lines originate in only a few of the several components contributing to the observed Fe II and Si II lines. However, we note that these b values are comparable to or lower than the b values obtained for systems for which we could fit the Zn II and Cr II lines directly. Furthermore, we have also used the weak lines of Fe II (which can be comparable in strength to the Zn II and Cr II lines) whenever available. In any case, we have also estimated the variation in the Zn II and Cr II column densities by varying the b values as explained below.

In cases where all the parameters were allowed to vary, the 1σ uncertainties in the parameters were computed simultaneously. In cases where the effective b values were assumed to be the same as those of Fe II or Si II lines, we determined the uncertainties in column densities, due to the uncertainty in b , by varying the effective b value by $\pm 1 \sigma$ as obtained for the Fe II or Si II lines used. We also investigated the effect of relaxing the constraints of same b value and same central velocity for lines of different ions i.e. Zn II, Cr II and Mg I and also, the effect of varying the Mg I column density (whenever it was taken from the SDSS data) to within its 1σ range. The reported errors in column density are inclusive of these effects, for all DLAs.

Table 5 lists the column densities and effective b values with 1σ errors, derived for the various heavy elements from our MMT data. The QSOs and redshifts are indicated by the same codes used in Table 2 and 4. We note that the column densities and the equivalent widths, obtained from them, for all individual lines of Zn and Cr are found to lie on the linear portion of the curve of growth. The column densities obtained are, therefore, only

marginally dependent on the b values and are not affected by line saturation. We note that this could partly arise from the large values of b which are the result of the resolution used for our observations and are indicative of multiple components. Although it is certainly desirable to obtain higher resolution observations in the future to resolve these components, the column densities obtained here should be close to the actual values (Jenkins 1986) unless there are hidden components with significant column density but extremely small b values.

Values of H I column densities, whenever available, and the column densities for some other ions, which were obtained from previously measured equivalent widths given in Table 2, are also included in Table 5.

4. Notes on Individual Objects

Q0738+313 [$z_{em}=0.630$; $z_{abs}=0.0912$, system A; $z_{abs}=0.2210$, system B] The spectrum in Fig. 1 shows Ti II and Ca II in system A, the Mg II doublet and a marginal detection of Mg I in system B. We also place limits on Be II λ 3131. The ionization potential of Ti II is close to that of H I, so $N_{\text{TiII}}/N_{\text{HI}}$ gives directly the abundance of titanium. For system A, assuming b for Ti to be the same as that for Ca, we get $\log(N_{\text{TiII}}/N_{\text{HI}})=-8.7$, giving $[\text{Ti}/\text{H}] < -1.6$. In this paper, we use the notation $[\text{X}/\text{H}]$ to mean the absolute logarithmic abundance of X with respect to hydrogen, including all forms of H and all forms of X, relative to the solar abundance. All the abundances given in this paper are upper limits because we do not take into account the possible presence of H_2 and H II, an assumption also made in all previous DLA abundance studies. Note that in high redshift DLAs $\text{H}_2/\text{H I}$ ratio has been observed to be small (e.g. Ledoux, Petitjean & Srianand 2003 and references therein), although such high H I columns are almost always accompanied by comparable H_2 in the Milky Way. There is a need to empirically determine the $\text{H}_2/\text{H I}$ ratio in low and intermediate DLAs, in order to study more precisely the redshift-abundance relation.

Interstellar Ca II lines arising in the Milky Way are seen in most spectra and are labeled “MW” in the plots.

For Ca II, the ionization potential is much lower than for H I, so ionization corrections are needed and the interpretation is more ambiguous than for Ti. The fact that the Ca II lines in the $z = 0.0912$ system are a little weaker than the Milky Way (MW) Ca II lines is consistent with the Ti depletion. The Routly Spitzer effect (Routly & Spitzer, 1952) normally exists in such MW sight lines, so the Ca II is not as depleted as in cold clouds. The calcium in system A may be as depleted as the titanium.

In the system B $[\text{Ti}/\text{H}] < -1.7$. The Mg II lines in this system are remarkably weak and

possibly indicate extreme saturation in individual, unresolved components. We thus get a lower limit on the Mg abundance as $[\text{Mg}/\text{H}] > -3.13$.

Q0827+243 [$z_{em}=0.941$; $z_{abs}=0.259$, system A; $z_{abs}=0.5249$, system B] System A shows only a weak Mg II system, similar in strength to that in the $z = 0.2209$ system in Q0738+313, but with strong evidence of saturation.

System B, of primary interest for this paper, contains strong lines $\lambda\lambda$ 2344, 2374, 2382, 2586, 2600 and weak lines $\lambda\lambda$ 2249, 2260 of Fe II; and lines $\lambda\lambda$ 2576, 2594 and 2606 of Mn II. A good limit is available for Fe I λ 2484. Multiple components are clearly indicated in the Fe II lines, with two dominant components separated by 50 km/sec. Column densities for both components are given in the table 5. Mn II lines also require two components with b values and central velocities very similar to those of Fe II lines. The 1σ errors in the b values for Mn II are, however, very large and so we take the b values to be same as that of the Fe II components. Single component fits require very large value of b (122 km s⁻¹) but give the same column density within the error bars.

We note that the limit on the ratio $N_{\text{FeI}}/N_{\text{FeII}}$ ($< 10^{-3}$) is comparable to the limits in our Galaxy in dense clouds: the radiation field in which the system B is immersed must be as effective in creating this low ratio as it is in the dense clouds in the disk of Milky Way.

Q0933+733 [$z_{em}=2.528$; $z_{abs}=1.479$, system A; $z_{abs}=1.4973$, system B; $z_{abs}=1.8283$, system C; $z_{abs}=1.8573$, system D; $z_{abs}=2.113$, system E; $z_{abs}=2.333$, system F; $z_{abs}=2.4500$, system G; $z_{abs}=2.5380$, system H] The primary system of interest for this paper is system A, which includes three, detectable, unblended lines of Ni II, the weakest permitted line of Si II, the doublet of Ti II, the doublet of Al III, the Zn II doublet and the Cr II triplet. From SDSS there is an upper limit of 0.3 Å on the rest equivalent width of the Mg I λ 2853 (Table 2). We obtain an upper limit of 13.6 mÅ on the equivalent width of Mg I λ 1827. The Si II λ 1808 yields a b value of 28.6 km s⁻¹. The b value obtained for Ni II $\lambda\lambda$ 1741, 1751 is also consistent with this b value within 1σ error. A good fit can be obtained for the Zn II, Cr II, Mg I and Ti II lines using this b value. The column density of Mg I, which is treated as a free parameter, is much smaller than the upper limit of 1.9×10^{13} cm⁻² obtained from the absence of 1827 line in our spectra and is also lower than the upper limit obtained from the equivalent width limit in Table 2. The Mg I column density is not well determined by the profile fit and the 1σ errors are much larger than the fitted value. We have, thus, only given the 3σ upper limit.

As for the other systems, systems C, D, G and H are seen only in C IV and not, for instance, in Si II (λ 1526) or Al II (λ 1670), the strongest lines of first ions in the observed spectral region. The absence of Al II in system C suggests that the possible Si II line of

system C, blended with Ni II λ 1741 of system A is of no consequence and that the line is fully Ni II of system A. System E is a multi-component system seen in C IV but also detected in Si IV and definitely not seen in Al II. System B is seen only in the Al III doublet, only 2200 km s⁻¹ from the same doublet in system A but showing no trace of the many other lines of system A, even though Al III is much stronger in system B than in system A.

System F has very strong C II, C IV, and Si IV; detectable Si II $\lambda\lambda$ 1526, 1304; excellent limits on Fe II λ 1608, $N_{\text{SiIII}}/N_{\text{FeII}} > 21.1$; but no detectable O I λ 1302: O I could be apparently missing because it is blended with Si IV in system E, but this is unlikely since the Si IV profile mimics well the multi-component C IV profile of the same system, showing no evidence of other structure that could be attributed to O I. System F is thus a purely ionized region, having high ions, of very low density, judging from the absence of CII* (observed wavelength 4451.9 Å). The absence of O I and C I in system F is in sharp contrast to the system B, in SDSSJ2340-0053 discussed below, in which O I is very strong in the presence of a similar set of ions.

There are two unidentified lines at 4515 and 5436 Å and possibly a third one at 5461 Å (blended with C IV in system H) which could most likely be the C IV 1548 line of additional systems at $z = 1.917, 2.511$ and 2.528 in which the C IV 1550 line is too weak to detect.

The remaining objects are quasars from the SDSS. Only SDSSJ1028-0100 has been observed before for absorption lines (Petitjean et al. 1998, hereafter P98). The objects are included in the DR1 list of QSOs (Schneider et al. 2002) The original SDSS spectra from which these objects were selected are on the public website: <http://skyserver.sdss.org/dr1/en/>. The catalog of lines found in SDSS is given by York et al. (2005a) and is partially included in Table 2. All the systems found below can either be identified in the SDSS spectra or are too weak to be detected in the SDSS QSO survey spectra. To use the website, the coordinates of the objects can be used, or one can use the plate and fiber numbers in Table 1.

SDSSJ 1028–0100 [$z_{em} = 1.542$; $z_{abs} = 0.324$, system A; $z_{abs} = 0.6321$, system B; $z_{abs} = 0.7088$, system C; $z = 1.265$, system D; $z_{abs} = 1.484$, system E] This QSO was observed by P98 (Q1026-0045B, in their paper) with HST, along with the nearby object Q1026-0045A ($z=1.438$)(SDSSJ 102835-010043.7).

Our data show system A to be a multicomponent Mg II system, with two Fe II lines in the observed range. The Fe II lines are weak and we infer $N_{\text{FeII}}/N_{\text{MgII}} = 2.02$. Mg I λ 2853 is present.

Systems B and C are the main systems of interest in this paper. The two systems are, interestingly, separated in z only by a little more than the two damped systems in SDSSJ1727 (Turnshek et al., 2004). Additional data are available from P98 as given in Table 2.

For system B, the Zn II and Cr II lines are in noisy part of the spectrum and we used the b value of Fe II lines for these lines. The column density of Mg I was obtained for this value of b from the λ 2853 line observed by the SDSS. The errors on the estimated column densities of Zn and Cr are large because of the poor quality of the spectrum in the region of interest. A good limit is obtained for Fe I λ 2484.

For system C Zn II λ 2026 and Mg I λ 2026 lines are blended with Si IV λ 1393 of system E. The λ 2056 line of Cr II is blended with λ 1550 line of C IV of system D. The b value for the Zn II and Cr II lines was assumed to be the same as that for Fe II. The column density of Mg I was obtained from the SDSS data for this value of b . Parameters for C IV lines of system D and Si IV lines of system E were obtained by fitting the unblended lines of these systems first. All the lines were then fitted together. Even though we were able to get the column density of Cr II reasonably well the column density of Zn II is poorly determined.

The HST spectrum for this QSO has become available recently (HST GO project No. 9382, P.I. Rao, S.). For both CDLAs the column densities are found to be close to 10^{20} cm^{-2} and the systems thus fall into the category of sub-DLAs. We have included our estimates of the H I column densities obtained by fitting the line profile to the HST data in Table 5. The 1σ errors in H I column densities were estimated to be ≈ 30 % taking into account the uncertainties in fitting the continuum. Because of the sub-DLA nature of these systems, we do not include them in our calculations presented in sections 5.2 and 5.4.

The pair of QSOs (Q1026-0045A and Q1026-0045B) contain several common systems (nearly identical redshifts), though they are separated by ~ 300 kpc. One is a pair of Lyman α /Lyman β systems at $z = 1.4439$ in object B and 1.4420 in object A, in which no lines of heavy elements are found. We have very good limits on Si IV, C IV, Al II, Si II and Al III: none of these features are seen to our limit of detection.

Another common pair is the system at $z = 1.265$ (our system D). Lyman α and Lyman β were seen in both objects. Si IV λ 1393 was detected in object A. We confirm the presence of strong C IV in the object B system, but can set stringent upper limits to the strengths of line of Al II, Si II and Al III. Evidently, this is a high ionization system, that must be larger than 300 kpc in transverse dimension as noted by P98. In object A, there is a separate absorber at $z = 1.2969$ which has O I, numerous first and second ions and Si IV. No lines are detected at this redshift in object B (our spectrum), so this is not a common pair.

System E was found (P98), in object B (not seen in object A), to have no first ions. It shows C IV and Si IV in the MMT spectrum, and N III, C III, Si III and possibly O VI in the spectrum from HST (P98). Again, no low ions (Al II, Si II) are present to strong

limits in the MMT spectrum, and Al III is not present. This is a low column density, highly ionized system.

We find one system, A, at $z = 0.324$ in Fe II $\lambda \lambda$ 2586, 2600. The other three, strong Fe II lines are clearly present in the P98 spectrum. One of these, and a weak C IV system at $z = 1.01$ led P98 to suggest, tentatively an Mg II doublet at $z = 0.11$: there is no evidence that this system is real as it is fully explained by the weak C IV doublet and our system A. Two lines of Fe II, two of Mg II and one of Mg I are detected. The lines of Fe II and Mg II are weak and we infer $N_{\text{FeII}}/N_{\text{MgII}}=2$.

In addition to the systems noted above, we can place stringent upper limits on any possible Al II for eleven Lyman α -only systems between $z = 0.96$ and 1.5.

SDSSJ 1107+0048 [$z_{em} = 1.302$; $z_{abs} = 0.7405$, system A; $z_{abs} = 1.0704$, system B; $z_{abs} = 1.3503$, system C; $z_{abs} = 1.3687$, system D] The prime system is A. In this system, two-components are present in Fe II, Zn II, and Cr II lines. For Fe II λ 2249 and Cr II λ 2066, a two-component fit gives the same column densities as does a single-component fit, with similar rms values for the fit. As there are too many variables for a two component fit of the Zn II, Cr II and Mg I lines, we used single components to get the column densities. The Mg I column density, which was treated as a free parameter, is consistent with the value from SDSS for the b value obtained here, within 1σ limits. Upper limits on Co II and Ti II are from the absence of λ 2012 and λ 1910 lines respectively. The HST spectrum for this QSO has become available recently (HST GO project No. 9382, P.I. Rao, S.). We have included our estimate of the H I column density obtained from the HST data in Table 5. The 1σ errors in H I column densities were estimated to be $\approx 30 \%$ taking into account the uncertainties in fitting the continuum.

System B contains only Al III and Al II, with comparable strengths. Systems C and D are weak C IV systems with no other lines detected.

SDSSJ 1323–0021 [$z_{em} = 1.390$; $z_{abs} = 0.7160$, system A; $z_{abs} = 1.3574$, system B; $z_{abs} = 1.3742$, system C; $z_{abs} = 1.3868$, system D; $z_{abs} = 1.3891$, system E]

System A, is the main system for our purpose, for which we have lines of Zn II, Cr II, and Fe II and limits on Co II. The λ 2056 line of Cr II is noisy and so can not be fitted to get the b value and the column density of Cr II. Therefore, the value of b is assumed to be the same as that of Fe II. The column density of Mg I is obtained from the SDSS data for this b .

Systems B, C, D and E are all C IV only systems, all within 4000 km/s of each other. For systems C, D and E, Si IV is in the observed range, but is below the detection limits.

The HST spectrum for this QSO has become available recently (HST GO project No. 9382, P.I. Rao, S.). We have determined the H I column density by fitting the line profile to the HST data and find it to be smaller than $2 \times 10^{20} \text{ cm}^{-2}$. The system thus falls into the category of sub-DLAs. We have included our estimate of the H I column density in Table 5. The 1σ errors in H I column densities were estimated taking into account the uncertainties in fitting the continuum. Because of the sub-DLA nature of this system, we do not include it in our calculations presented in sections 5.2 and 5.4.

SDSSJ 1727+5302 [$z_{em} = 1.444$; $z_{abs} = 0.9449$, system A; $z_{abs} = 1.0311$, system B; $z_{abs} = 1.2565$, system C; $z_{abs} = 1.3064$, system D] Systems A and B are the prime systems for this paper. These systems reveal weak lines of Ni II, Al III, Si II, Cr II and Zn II. Ti II is detected in system A. A strong line is present at the position $\lambda 1941$ of Co II. However, the line $\lambda 2012$ of Co II, having comparable f value, is absent and so this line must be a blend. Limits are placed on Ti II and Co II column densities in system B. For system A, the column density of Mg I that we get by fitting our data is consistent within 1σ with the value obtained from SDSS data, within error bars. Other singly ionized species also give b values similar to Zn II, Cr II, Mg I lines. For system B a good fit is obtained for b value close to those of the other singly ionized lines. Mg I is taken from the SDSS value.

For systems A and B we adopt the H I column densities given by Turnshek et al. (2004) but allow for 30% error in these values in light of the confusing region (Lyman beta emission line) in which the damped systems appear and the several choices of continuum that are possible for the region.

Systems C and D are weak, C IV-only systems.

SDSSJ 2340–0053 [$z_{em} = 2.085$; $z_{abs} = 1.3606$, system A; $z_{abs} = 2.0547$, system B; $z_{abs} = 2.062$, system C] System A is the prime system for this study. In this system, we detect Al II, Ni II, Si II ($\lambda 1808$), Zn II, Cr II and Fe II. The Mg I column density obtained here is consistent with the SDSS value within the 1σ error. A limit is obtained for Al I $\lambda 2263$.

System B has a broad range of ionization states represented, from C I to C IV. System C has only C IV and is separated by only 200 km/sec from B, so the two systems are probably associated with each other and with the quasar. Note that the strong O I line indicates that three regions of different ionizations are involved in system B/C: an H I region (dominant in H I and O I with traces of the C I and presumably with Si II, C II and Al II); and an H II region, possibly with a wide range of ionization (C II, C IV, Si II, Si IV, Al II, Al III); and a highly ionized region, system C, with C IV only (and no Si IV in particular). The fine structure excited line, C II* $\lambda 1335$ may be present, but it is ambiguous whether it is from

the H I region, the H II region, or both. The system is similar to what one sees looking from afar at a QSO through Loop I (Burkes et al. 1991) and the Milky Way. The C I line at 5060 Å shows evidence of the C I* and C I** components, implying significant densities in the H I region. The H I region may be a good candidate for detecting molecular hydrogen: the ratio $N_{\text{SiIII}}/N_{\text{FeII}}$ is low, as in cold cloud gas in our Galaxy, indicating the presence of grains, and the neutral gas is cold. These are the main conditions for forming H₂ (Tumlinson et al. 2002). On the other hand, the Cl I 1347 line, formed by charge exchange between Cl⁺ and H₂ and normally strong in H₂-containing clouds in our Galaxy (Jura & York 1978), is not present. Either the overall abundance of Cl is low, or the amount of H₂ is low, or both.

5. Results

5.1. Relative Abundances

Table 6 lists the abundances of Cr, Fe, Ni, Al, Si, Ti, Mn, and Co relative to Zn, and Si relative to Fe, for the systems in our sample. We have used solar system abundances from Lodders (2003) as a reference. The table also lists the averages of these relative abundances as well as the average values obtained for the compilation of Prochaska et al. (2003a) for DLAs at $z > 2.5$. The values for Galactic warm clouds, cold clouds and halo clouds, taken from Welty et al. (1997,1999a,1999b,2001) and York et al. (2005b) are also included for comparison.

The relative abundances of various elements are determined both by the nucleosynthetic processes and by the differential dust depletion. If the abundance pattern resembles that of Galactic halo stars, the α elements such as Mg, Si, S, O, Ar may be nucleosynthetically enriched compared to the iron group elements such as Cr, Mn, Fe, Co, Ni and Zn (because the former are produced by Type II supernovae). The odd-Z elements such as Al and Mn may be deficient compared to even-Z elements such as Si and Fe, respectively. Furthermore, the refractory elements such as Si, Ti, Cr, Mn, Fe, Co, and Ni are expected to be depleted if the DLAs contain dust. We use Zn as the reference element because, as noted before, it is almost undepleted in warm Galactic interstellar clouds and shows relatively small depletion even in cold Galactic interstellar clouds. $[\text{Cr}/\text{Zn}]$ is a measure of the amount of dust, and we discuss it in detail in the next subsection.

For both sub-DLAs toward SDSS1028-0100, the errors in Zn II column densities are large. We, therefore, use the 3σ upper limits on the Zn II column density and give lower limits to the abundances of various elements w.r.t. Zn for these systems. The average values of relative abundances as measured by us are very similar to the values obtained by

Prochaska et al (2003a) at redshifts > 2.5 , suggesting that the nature and amount of dust in DLAs do not vary much with redshift.

For $[\text{Si}/\text{Zn}]$ Prochaska et al. (2003a) have reported only one measurement of 0.08. Even though this is different from the average value obtained by us, it is well within the spread of our values. Overall our values, together with those compiled by Ledoux, Bergeron & Petitjean (2002a), Prochaska et al. (2003a) and Dessauges-Zavadsky, Prochaska & D’Odorico (2002) (a total of 18 in all), show $[\text{Si}/\text{Zn}]$ to be in the range of -0.8 to +0.2. If the depletion pattern in DLAs is similar to that in the warm Galactic clouds, these values indicate super-solar total abundance of Si by a factor of 2 or larger in only 3 of these systems.

Welty et al. (2001) note, however, that $[\text{Si}/\text{Zn}]$ is solar in the gas in the Small Magellanic Cloud (SMC) toward the star Sk 155, with a so-called SMC extinction curve. Other stars in the SMC show the same effect (Welty et al. in preparation), even though $[\text{Fe}/\text{Zn}]$ is subsolar in the same sight lines. Thus, one must allow for the possibility that the grain composition differs from place to place and that Si is just not depleted much in some cases. In that case, the abundance of Si may not be as high as noted above.

Ti has been observed in very few DLAs so far. Dessauges-Zavadsky et al. (2002) and Prochaska et al. (2003a) have reported one value each, 0.29 and -0.94, respectively, for $[\text{Ti}/\text{Zn}]$, while the average of 5 values compiled by Ledoux et al. (2002a) is -0.26. We measure $[\text{Ti}/\text{Zn}]$ in two systems. Altogether, only 3 out of 9 of these values indicate super-solar abundance by a factor of 2 or larger, assuming the depletion to be similar to that in warm Galactic clouds. This suggests that α enrichment by type II supernovae may not be important in a large fraction of the DLAs.

We have measured the column densities of Al II and Al III in two systems which have Zn measurements. For one of these we also have an upper limit on Al I which is much smaller than the column densities of the other Al ions. Thus we have $[\text{Al}/\text{Zn}] = -1.2$ and -0.6 for $z = 1.03$ DLA in SDSSJ1727+5302 and $z = 1.36$ DLA in SDSSJ2340-0053 respectively. This suggests dust depletion in these DLAs, irrespective of whether the intrinsic nucleosynthetic pattern is similar to the solar pattern or that observed in halo stars (e.g. Lauroesch et al. 1996; Kulkarni, Fall & Truran 1997). However, we note that Al II lines are strong and may possibly be saturated, in which case these values should, strictly, be treated as lower limits.

We have measured $[\text{Mn}/\text{Zn}]$ in one system to be -0.6. The average of 9 values compiled by Ledoux et al. (2002a) is -0.66 and that of the three values reported by Dessauges-Zavadsky et al. (2002) is -0.77. All these values suggest moderate to high depletion for the solar abundance pattern as well as the halo-star abundance pattern.

The values of $[\text{Ni}/\text{Zn}]$ obtained by us indicate substantial depletion for the solar abun-

dance pattern as well for the halo-star abundance pattern.

5.2. Redshift Evolution of Dust Content

The $[\text{Cr}/\text{Zn}]$ values for our sample are similar to the $[\text{Cr}/\text{Zn}]$ values found at high redshifts. To make a quantitative comparison, we combined our data with data from the literature. We examined the data of Boisse et al. (1998); Centurion et al. (2003), Dessauges-Zavadsky et al. (2003, 2004); de La Varga et al. (2000); Ellison & Lopez (2001); Ge, Bechtold, & Kulkarni (2001); Ledoux, Srianand, & Petitjean (2002b); Ledoux, Petitjean, & Srianand (2003); Lu et al. (1995, 1996); Lopez et al. (1999, 2002); Lopez & Ellison (2003); Meyer & York (1992); Meyer, Lanzetta, & Wolfe (1995); Molaro et al. (2000); Péroux et al. (2002); Petitjean, Srianand, & Ledoux (2000, 2002); Peroux et al. (2002); Pettini et al. (1994, 1997, 1999, 2000); Prochaska & Wolfe (1996, 1997, 1998, 1999, 2000); Prochaska, Gawiser & Wolfe (2001a), and Prochaska et al., (2001b, 2003a, 2003b, 2003c). To be conservative, we excluded sub-DLAs ($10^{19} \text{ cm}^{-2} N_{\text{HI}} < 2 \times 10^{20} \text{ cm}^{-2}$) and the systems separated by $< 3000 \text{ km s}^{-1}$ from the QSO redshift. We, also, excluded cases where only upper or lower limits are available for Cr and/or Zn, and scaled the measurements to the same set of oscillator strengths for the Zn II and Cr II lines which are given in Table 3. In Fig. 9, we plot $[\text{Cr}/\text{Zn}]$ vs. redshift for this combined sample of 41 DLAs. Our MMT data have provided 4 new $[\text{Cr}/\text{Zn}]$ measurements for DLAs at $z < 1.5$ and nearly doubled the existing sample of $[\text{Cr}/\text{Zn}]$ measurements at these redshifts. In addition our MMT data have provided $[\text{Cr}/\text{Zn}]$ ratio for two CDLAs and two sub-DLAs which are also shown in Fig. 9.

A linear regression fit to the unbinned $[\text{Cr}/\text{Zn}]$ vs. redshift data gives a slope of 0.07 ± 0.01 , and an intercept of -0.48 ± 0.02 implying a slow decrease in $[\text{Cr}/\text{Zn}]$ with decreasing redshift. The linear correlation coefficient between $[\text{Cr}/\text{Zn}]$ and z is 0.19.

To examine the extent to which the above conclusion is affected by the scatter among the individual $[\text{Cr}/\text{Zn}]$ values, we also binned the data into six redshift bins with roughly equal number of systems per redshift bin. The unweighted mean $\langle [\text{Cr}/\text{Zn}] \rangle$ in each bin vs. the median redshift of the bin is plotted in Fig. 10a. The vertical error bar for each bin denotes the 1σ uncertainty in the unweighted mean, and includes the sampling uncertainties as well as the measurement uncertainties calculated by propagating the errors in individual Cr and Zn measurements. Linear regression for the mean $[\text{Cr}/\text{Zn}]$ vs. redshift gives a slope of -0.03 ± 0.06 , an intercept of -0.26 ± 0.13 , and a linear correlation coefficient of -0.18 .

To examine the evolution of “global depletion”, we define the N_{ZnII} -weighted mean $\langle [\text{Cr}/\text{Zn}] \rangle \equiv \log(\Sigma N_{\text{CrII}}^i / \Sigma N_{\text{ZnII}}^i) - \log(\text{Cr}/\text{Zn})_{\odot}$. Note that $\Sigma N_{\text{CrII}}^i / \Sigma N_{\text{ZnII}}^i$ corresponds to

$\Omega_{\text{Cr}}/\Omega_{\text{Zn}}$, Ω_{Cr} and Ω_{Zn} being the mean comoving density of Zn and Cr, respectively, in units of the critical energy density of the universe. Fig. 10b shows this weighted mean $[\langle \text{Cr}/\text{Zn} \rangle]$ vs. median redshift in each bin for our combined sample. The vertical error bar for each bin denotes the 1σ uncertainty in the weighted mean, and includes the sampling uncertainties as well as the measurement uncertainties. The procedures for calculating these uncertainties are similar to those employed in Kulkarni & Fall (2002). Linear regression analysis for this N_{ZnII} -weighted mean depletion vs. redshift gives a slope of 0.05 ± 0.06 , an intercept of -0.41 ± 0.12 , and a linear correlation coefficient of 0.32.

The intercept value for the N_{ZnII} -weighted mean depletion is negative at $\approx 3.3\sigma$ level, suggesting that the mean global dust depletion of DLAs is significant at all redshifts examined ($0.6 < z < 3.4$). However, the slope values are consistent with zero. Overall, we conclude that the existing data do not suggest much evolution of the conventional dust content indicator, $[\text{Cr}/\text{Zn}]$ in DLAs with redshift. Recently Vladilo (2004) has found evidence for an increase of dust-to-gas ratio with increasing metallicity, using $[\text{Fe}/\text{Zn}]$ in 38 DLAs, but has found only a weak evidence for the evolution of this ratio with time.

5.3. Quasar Reddening and Element Depletions

If the observed depletions of elements such as Cr or Fe relative to Zn are caused by dust in the DLAs, the spectra of background quasars may be expected to be reddened by the intervening dust. Pei, Fall, & Bechtold (1991) found the spectra of quasars with DLAs to be systematically reddened with respect to the spectra of quasars without DLAs. Similar study with a much larger, homogeneous sample of QSOs from the SDSS DR2 by Murphy and Liske (2004) has found no evidence for such reddening at the redshift of about 3. However, the dust effects are likely to be more important at the lower redshifts sampled by our DLAs. Although our sample is small, it consists of strong DLAs or CDLAs. Therefore, it is interesting to ask whether the quasars in our sample are systematically more reddened than a typical quasar without a foreground DLA. To address this, we focus on the SDSS objects in our sample, for which a uniform set of measurements are available for the quasar spectral and photometric properties. Below we make a preliminary search for correlations between the quasar reddening and $[\text{Cr}/\text{Zn}]$ in the absorbers, using two different estimates of the reddening based on (a) the shape of the quasar spectrum, and (b) the quasar $g - i$ color.

5.3.1. Reddening Estimates based on Quasar Spectra

Reichard et al. (2003) have constructed a composite quasar spectrum using 3,814 spectra from the SDSS EDR. They have also fitted the spectra of the individual EDR quasars to the composite spectrum, assuming that the continuum follows a power law $f_\nu \propto \nu^\alpha$, that is diminished by dust extinction characterized by reddening $E(B - V)$. They assume the reddening law for the SMC from Pei (1992). Table 7 lists, for the SDSS quasars in our sample, the best-fitting values of the spectral index α_{RP} and the reddening $E(B - V)_{RP}$ as found by Reichard et al. (private communication). Here, R stands for reddening law and P for power law, both of which were used to determine these parameters. Also listed in Table 7 are qualitative comments about the colors of the quasars based on visual inspection of the spectra. But we note that there is a degeneracy between the values of α_{RP} and $E(B - V)_{RP}$, i.e. several combinations of the two fit parameters can provide almost equally satisfactory fits. As a result, the α_{RP} and $E(B - V)_{RP}$ values sometimes have unphysically high or low values. For this reason, reliable values of α_{RP} and $E(B - V)_{RP}$ are not available for SDSSJ1028-0100. Two of the remaining quasars (SDSSJ1107+0048 and SDSSJ2340-0053) are not significantly reddened, and show $E(B - V)_{RP}$ consistent with the SDSS composite for “flat-spectrum” quasars (sample 1 of Richards et al. 2003). The remaining two quasars (SDSSJ1323-0021 and SDSSJ1727+5302) have higher values of $E(B - V)_{RP}$.

5.3.2. Reddening Estimates Based on Quasar Colors

We also attempted to constrain the reddenings in another way for the SDSS quasars, since the $E(B - V)_{RP}$ values may not always be the best physical indicators of the actual reddening. To do this, we used the observed $g - i$ colors of the quasars and calculated the excess $\Delta(g - i) \equiv (g - i) - (g - i)_{med}$, where $(g - i)_{med}$ is the median $g - i$ color for the SDSS quasar composite at the redshift of the quasar, taken from Table 3 of Richards et al. (2001). We then use the SMC reddening law, $A_\lambda = 1.39\lambda^{-1.2}E(B - V)$ (Prevot et al. 1984) to obtain the $E(B - V)_{g-i}$ from the observed $\Delta(g - i)$ values. Taking λ_g and λ_i to be 4657.98 Å and 7461.01 Å respectively, this gives $E(B - V)_{g-i} = \Delta(g - i)(1 + z)^{1.2}/1.506$, z being the redshift of the absorber. To obtain the $E(B - V)$ for individual DLAs toward SDSSJ1727+5302 we assumed them to be in proportion to the H I column densities in these systems. The $E(B - V)_{g-i}$ values are given in Table 7.

5.3.3. Search for Correlations between Reddening Estimates and DLA Depletions

It is not clear whether the reddening in any of our targets (estimated by either of the above methods) is caused by dust intrinsic to the quasar or dust in the intervening absorbers. Indeed, the 2200 Å bump has been observed in a few quasar spectra at the redshifts of the quasar and/or the intervening absorbers (Wang et al. 2004). Hopkins et al. (2004), using SDSS data, have shown the reddening to be dominated by SMC type dust at the QSO redshifts. In any case, the observed $E(B - V)_{RP}$ or $E(B - V)_{g-i}$ values can be used to constrain the amounts of reddening that could be caused by the intervening DLAs. From these, assuming the $E(B - V)$ to be caused by the DLA absorber and assuming it to be equal to N_{HI}/D (ignoring possible presence of H_2) one can either obtain the H I column densities in the absorbers assuming a value of the constant D for a specific extinction curve, or obtain the value of D if N_{HI} is known. These column densities, together with the observed Zn II column densities, can then be used to constrain the metallicities for the DLAs for which N_{HI} is not yet known. Table 8 lists the N_{HI} values inferred from HST spectra (where available), along with estimates of N_{HI} from the reddening $E(B - V)_{g-i}$, assuming $D = 4.6 \times 10^{22} \text{ cm}^{-2} \text{ mag}^{-1}$ for the SMC extinction curve. The table also includes the corresponding values/estimates of the abundances of Zn and Ti. We note, however, that the H I column densities obtained from the $E(B - V)$ values for SDSS1107+0048 and SDSS1323-0021 differ considerably from their HST values. The H I column densities obtained from the $E(B - V)$ can, therefore, only be taken to be tentative values. We, thus, do not include the metallicity obtained in this manner for SDSSJ2340-0053 in our calculations for metallicity evolution, presented in the next subsection. Using the HST values of H I column densities we get the values for D of 2.0×10^{22} , 1.0×10^{21} and 1.1×10^{23} for the DLAs in SDSS1107+0048, SDSS1323-0021 and SDSS 1727+5302 respectively.

Fig. 11 plots the two estimates of reddening for the SDSS quasars in our sample vs. the $[\text{Cr}/\text{Zn}]$ in the corresponding DLAs. The circles show the $E(B - V)_{RP}$ values while the squares show the $E(B - V)_{g-i}$ values. The filled symbols are for quasars with single DLAs, while the unfilled symbols are for a quasar (SDSSJ1727+5302) with two DLAs along the line of sight, treated as described above to estimate the individual contributions of the two systems. There may be some anti-correlation between $[\text{Cr}/\text{Zn}]$ and the reddening, such as may be expected if the reddening arises primarily in the absorbers, and the absorbers with the higher depletion of Cr are also the ones with the greater reddening, and vice versa. The correlation is less clear if the double sight line is included, but the reddening estimates for such absorbers are less certain because of the assumption of the same extinction law for both systems in the sight line. Clearly, it is necessary to obtain element depletions in many more SDSS sight lines and to employ more robust estimators of the reddening to determine whether the correlation possibly present in Fig. 11 is truly significant.

5.4. Constraints on Metallicities and Implications for Metallicity Evolution

Finally, we study the implications of our MMT data for the metallicity evolution of DLAs. The analysis presented here is based on the methodology outlined in Kulkarni & Fall (2002) and uses the data compiled therein along with the more recent data referred to in section 5.2 as well as the data presented in this paper. We binned the combined sample in redshift and calculated the global N_{HI} -weighted metallicity in each bin.

The last two columns of Table 8 give the estimated abundances of Zn and Ti. In most systems the abundances of Zn and Ti are smaller than a tenth of the corresponding solar abundances except in the case of SDSS1323-0021, for which the Zn abundance has a very high value.

For the sample of 41 DLAs mentioned above (section 5.2), the N_{HI} -weighted mean metallicity in the $0.7 < z < 1.5$ range is -1.09 ± 0.20 , and the linear regression slope of the metallicity-redshift relation is -0.21 ± 0.10 for the redshift range $0.7 < z < 3.4$. Considering only Zn measurements, irrespective of whether or not Cr was measured, a total of 83 DLAs (51 detections, 32 limits) are currently available from our MMT data and data from the literature. We constructed two samples for these 83 DLAs: a “maximum limits” sample where the Zn limits are treated as detections, and a “minimum limits” sample, where the Zn limits are treated as zeros. For an individual system these extreme cases cover the full range of possible values the Zn column densities can take in the case of the limits. The N_{HI} -weighted mean metallicity in the redshift range $0.4 < z < 1.5$ is -1.03 ± 0.14 for both the “maximum limits” sample and the “minimum limits” samples. The linear regression slope of the metallicity-redshift relation for the redshift range $0.4 < z < 3.9$ is -0.13 ± 0.08 for the “maximum limits” sample, and -0.27 ± 0.10 for the “minimum limits” sample. The corresponding estimates for the intercept of the metallicity-redshift relation are -0.87 ± 0.19 for the “maximum limits” sample and -0.66 ± 0.22 for the “minimum limits” sample.

Thus our data seem to indicate that there is no strong evolution of the global metallicity with redshift. We note that we have only one value at $z < 0.6$ in our data set. Measurements at lower redshifts are important for better determination of the global metallicity evolution. Kulkarni et al. (2004) have taken steps in this direction by obtaining HST data at $z < 0.6$.

6. Discussion

The issues of dust depletion and associated selection effects, and the evolution of metallicity in DLAs are not yet fully understood. The large samples of DLAs or CDLAs becoming available from the SDSS can be used to improve the statistics of both element abundances

and dust reddening. In this paper, we have presented results for 7 CDLAs discovered in the SDSS and have doubled the Zn and Cr samples at $z < 1$. Our data suggest weak evolution of metallicity and dust content in the absorbers with redshift.

Kulkarni & Fall (2002), using 57 Zn measurements in the redshift range $0.4 < z < 3.4$, found the slope of the N_{HI} -weighted mean metallicity-redshift relation to be -0.26 ± 0.10 . A very similar value of the slope was also obtained by Prochaska et al. (2003b) using metallicity estimates for 121 DLAs with $0.5 < z < 4.7$. Ten of these are based on Zn, six on Fe (corrected by adding an assumed level of dust depletion), one on the X-ray absorption, and the remaining on Si, S, or O. The estimates of the metallicity-redshift relation presented in our study are also consistent with both of these results.

We note that we have used only Zn as a tracer of metallicity for several reasons: (a) This avoids complications (present in the case of Si, S, or O) of significant nucleosynthetic differences from the common metallicity indicator Fe. (b) Zn allows direct metallicity estimates nearly free from dust depletion corrections which can be significant for Fe. (c) The use of one element also makes the study of metallicity evolution more uniform. Nevertheless, it is very interesting that results based on Zn alone agree with those based on other elements.

We also note that out of the 121 DLAs in the sample of Prochaska et al. (2003b), only 9 have $z < 1.5$. Furthermore, the metallicity estimate for the lowest redshift system in that sample ($z = 0.52$) is based on X-ray absorption measurement of Junkkarinen et al. (2004), not on Zn, and there could be systematic differences between metallicity estimates based on Zn and those based on X-ray absorption. Thus, our MMT measurements at $0.6 < z < 1.5$ are a significant addition to the existing abundance data at intermediate redshifts.

In a recent study, Nestor et al. (2003) have averaged SDSS spectra at the positions of the Zn II and Cr II lines, all deredshifted to the rest frame of the absorber, as found from the Mg II lines. They found $[\text{Cr}/\text{Zn}] = -0.44 \pm 0.13$ at redshifts averaged from 0.9 to 2.2. These values are similar to the values in the literature, summarized above, and also with our values obtained from the analysis of individual spectra of SDSS objects. However, the variation of the ratio $[\text{Cr}/\text{Zn}]$ from system to system is large, as we confirm here for $z < 1.5$, and as has been observed for $z > 1.5$. It is important to determine if this variation is caused by a variation in the dust-to-gas ratio and if that correlates with variation in the extinction.

Overall, our observations have demonstrated the potential of the SDSS, combined with higher resolution follow-up spectra, to study the chemical evolution of the DLAs. Further studies of a large number of SDSS DLAs at $z < 1.5$ will help to determine the low- z end of the cosmic metallicity-redshift relation to a much higher accuracy than before. Such studies will help to understand whether or not DLA observations agree with predictions of cosmic

chemical evolution models, and whether dust extinction effects are significant.

We are grateful to the staff at the MMT for technical assistance. We also thank T. Reichard, P. Hall, and G. Richards for discussions about reddening for the SDSS quasars. PK acknowledges travel support from the Inter-University Center for Astronomy and Astrophysics, Pune and the use of computational facilities at the Institute of Physics, Bhubaneswar. VPK and JTL acknowledge partial support from the NASA / Space Telescope Science Institute grant GO-9441. VPK also acknowledges partial support from the National Science Foundation grant AST-0206197. PK and VPK also acknowledge partial support from the University of South Carolina Research Foundation.

Facilities: MMT(Blue channel spectrograph).

REFERENCES

- Abazajian, K. et al. 2003, *AJ*, 126, 2081
- Bartelman, M., & Loeb, A. 1996, *ApJ*, 457, 529
- Bergeson, S. D., & Lawler, J. E. 1993a, *ApJ*, 414, L137
- Bergeson, S. D., & Lawler, J. E. 1993b, *ApJ*, 408, 382
- Bergeson, S. D., Mullman, K. L., & Lawler, J. E. 1994, *ApJ*, 435, 157
- Bergeson, S. D., Mullman, K. L., Wickliffe, M. E., Lawler, J. E., Litzen, U., & Johansson, S. 1996, *ApJ*, 464, 1044
- Boissé, P., Boulade, O., Kunth, D., Tytler, D., & Vigroux, L. 1992, *A&A*, 262, 401
- Boissé, P., Le Brun, V., Bergeron, J., & Deharveng, J.-M. 1998, *A&A*, 333, 841
- Burks, G., York, D. G., Blades, J. C., Bohlin, R. C., & Wamsteker, W. 1991, *ApJ*, 381, 55
- Centurion, M., Molaro, P., Vladilo, G., Peroux, C., Levshakov, S. A., & D’Odorico, V. 2003, *A&A*, 403, 55
- de la Varga, A., Reimers, D., Tytler, D., Barlow, T., & Burles, S. 2000, *A&A*, 363, 69
- Dessauges-Zavadsky, M., Calura, F., Prochaska, J. X., D’Odorico, S. & Matteucci, F. 2004, *A&A*, 416, 79

- Dessauges-Zavadsky, M., Peroux, C., Kim, T.-S., D’Odorico, S., & McMahon, R. G., 2003, MNRAS, 345, 447
- Dessauges-Zavadsky, M., Prochaska, J. X., & D’Odorico, S. 2002, A&A, 391, 801
- Ellison, S. L., & Lopez, S. 2001, A&A, 380, 117
- Fall, S. M., & Pei, Y. C. 1993, ApJ, 402, 479
- Fukugita, M., Ichikawa, T., Gunn, J. E., Doi, M., Shimasaku, K., & Schneider, D. P. 1996, AJ, 111, 1748
- Ge, J., Bechtold, J., & Kulkarni, V. P. 2001, ApJ, 547, L1
- Glazebrook, K. et al. 2003, ApJ, 587, 55
- Gunn, J. E. et al. 1998, AJ, 116, 3040
- Hopkins, P. F. et al. 2004, AJ, in press, astro-ph/0406293
- Jenkins, E. B. 1986, ApJ, 304, 739
- Junkkarinen, V. T., Cohen, R. D., Beaver, E. A., Burbidge E. M., Lyons, R. W., & Madejski, G. 2004, ApJ, in press
- Jura, M., & York, D. G. 1978, ApJ, 219, 861
- Kulkarni, V. P., Fall, S. M., & Truran, J. W. 1997, ApJ, 484, L7
- Kulkarni, V. P., & Fall, S. M. 2002, ApJ, 580, 732
- Kulkarni, V. P., Hill, J. M., Shneider, G., Weymann, R. J., Storrie-Lombardi, L. J., Rieke, M. J., Thompson, R. I., & Jannuzi, B. T. 2001, ApJ, 551, 37
- Kulkarni, V. P., Fall, S. M., Lauroesch, J. T., York, D. G., Welty, D. E., Khare, P., & Truran, J. W. 2004, ApJ, submitted
- Lauroesch, J. T., Truran, J. W., Welty, D. E., & York, D. G. 1996, PASP, 108, 641
- Ledoux, C., Bergeron, J., & Petitjean, P. 2002a, A&A, 385, 802
- Ledoux, C., Srianand, R., & Petitjean, P. 2002b, A&A, 392, 781
- Ledoux, C., Petitjean, P., & Srianand, R. 2003, MNRAS, 346, 209
- Lilly, S. J., Le Fevre, O., Hammer, F., & Crampton, D. 1996, ApJ, 460, 1

- Lodders, K. 2003, *ApJ*, 591, 1220
- Lopez, S., & Ellison, S. L. 2003, *A&A*, 403, 573
- Lopez, S., Reimers, D., Rauch, M., Sargent, W. L. W., & Smette, A. 1999, *ApJ*, 513, 598
- Lopez, S., Reimers, D., D’Odorico, S., & Prochaska, J. X. 2002, *A&A*, 385, 778
- Lu, L., Sargent, W. L. W., Barlow, T. A., Churchill, C. W., & Vogt, S. S. 1996, *ApJS*, 107, 475
- Lu, L., Savage, B. D., Tripp, T. M., & Meyer, D. M. 1995, *ApJ*, 447, 597
- Madau, P., Ferguson, H. C., Dickinson, M. E., Giavalisco, M., Steidel, C. C., & Fruchter, A. 1996, *MNRAS*, 283, 1388
- Malaney, R. A., & Chaboyer, B. 1996, *ApJ*, 462, 57
- Meyer, D. M., Lanzetta, K. M., & Wolfe, A. M. 1995, *ApJ*, 451, L13
- Meyer, D. M., & York, D. G. 1992, *ApJ*, 399, L121
- Mishenina, T. V., Kovtyukh, V. V., Soubiran, C., Travaglio, C., & Busso, M. 2002, *A&A*, 396, 189
- Molaro, P., Bonifacio, P., Centurin, M., D’Odorico, S., Vladilo, G., Santin, P., & Di Marcantonio, P. 2000, *ApJ*, 541, 54
- Morton, D. C. 2003, *ApJS*, 149, 205
- Murphy, M. T., & Liske, J. 2004, *MNRAS*, submitted, astro-ph/0405472
- Nestor, D. B., Rao, S. M., Turnshek, D. A., & Vanden Berk, D. 2003, *ApJ*, 595, L5
- Pei, Y. C., Fall, S. M., & Bechtold, J. 1991, *ApJ*, 378, 6
- Pei, Y. C. 1992, *ApJ*, 395, 130
- Pei, Y. C., & Fall, S. M. 1995, *ApJ*, 454, 69
- Pei, Y. C., Fall, S. M., & Hauser, M. G. 1999, *ApJ*, 522, 604
- Peroux, C., Petitjean, P., Aracil, B., & Srianand, R. 2002, *NewA*, 7, 577
- Petitjean, P., Srianand, R., & Ledoux, C. 2000, *A&A*, 364, L26

- Petitjean, P., Srianand, R., & Ledoux, C. 2002, MNRAS, 332, 383
- Petitjean, P., Surdej, J., Smette, A., Shaver, P., Muecket, J., & Remy, M. 1998, A&A, 334, 45
- Pettini, M., Smith, L. J., Hunstead, R. W., & King, D. L. 1994, ApJ, 426, 79
- Pettini, M., Ellison, S. L., Steidel, C. C., & Bowen, D. V. 1999, ApJ, 510, 576
- Pettini, M., Ellison, S. L., Steidel, C. C., Shapley, A. E., & Bowen, D. V. 2000, ApJ, 532, 65
- Pettini, M., King, D. L., Smith, L. J., & Hunstead, R. W. 1997, ApJ, 478, 536
- Prevot, M. L., Lequeux, J., Maurice, E., Prevot, L., & Rocca-Volmerange, B. 1984, A&A, 132, 389
- Prochaska, J. X., Castro, S., & Djorgovski, S. G. 2003c, ApJS, 148, 317
- Prochaska, J. X., Gawiser, E., & Wolfe, A. M. 2001a, ApJ, 552, 99
- Prochaska, J. X., Gawiser, E., Wolfe, A. M., Cooke, J., & Gelino, D. 2003a, ApJS, 147, 227
- Prochaska, J. X., & Wolfe, A. M. 1996, ApJ, 470, 403
- Prochaska, J. X., & Wolfe, A. M. 1997, ApJ, 474, 140
- Prochaska, J. X., & Wolfe, A. M. 1998, ApJ, 507, 113
- Prochaska, J. X., & Wolfe, A. M. 1999, ApJS, 121, 369
- Prochaska, J. X., & Wolfe, A. M. 2000, ApJ, 533, L5
- Prochaska, J. X., & Wolfe, A. M. 2002, ApJ, 566, 68
- Prochaska, J. X. et al. 2001b, ApJS, 137, 21
- Prochaska, J. X., Gawiser, E., Wolfe, A. M., Castro, S., & Djorgovski, S. G. 2003b, ApJ, 595, L9
- Rao, S. M., Nestor, D. B., Turnshek, D. A., Lane, W. M., Monier, E. M., & Bergeron, J. 2003, ApJ, 595, 94
- Rao, S. M., & Turnshek, D. A. 2000, ApJS, 130, 1
- Reichard, T. A. et al. 2003, AJ, 126, 2594

- Reichard, T. A. et al. 2001, *AJ*, 121, 2308
- Richards, G. T. et al. 2002, *AJ*, 123, 2945
- Richards, G. T. et al. 2003, *AJ*, 126, 1131
- Routley, P. M., & Spitzer, L. Jr. 1952, *ApJ*, 115, 227
- Ryan, S. G., Norris, J., E., & Beers, T. C. 1996, *ApJ*, 471, 254
- Savage, B. D., & Sembach, K. R. 1996, *ARAA*, 34, 279
- Savaglio, S. 2001, in *The Extragalactic Infrared Background and its Cosmological Implications*, IAU Symposium, 204, ed. M. Harwit & M. G. Hauser, (ASP: San Francisco), 24
- Schneider, D. P. et al. 2002, *AJ*, 123, 567
- Somerville, R. S., Primack, J. R., & Faber, S. M. 2001, *MNRAS*, 320, 504
- Steidel, C. C., & Sargent, W. L. W. 1992, *ApJS*, 80, 1
- Stoughton, C. et al. 2002, *AJ*, 123, 485
- Strauss M. A. et al, 2004, *AJ*, in press
- Tissera, P. B., Lambas, D. G., Mosconi, M. B., & Cora, S. 2001, *ApJ*, 557, 527
- Tumlinson, J. et al. 2002, *ApJ*, 566, 857
- Turnshek, D. A., Rao, S. M., Nestor, D. B., Vanden Berk, D., Belfort, M., & Monier, E. M. 2004, *ApJ*, in press, astro-ph/0404609
- Ulrich, M.-H., & Owen, F. N. 1977, *Nature*, 269, 673
- Veron-Cetty, M. P., & Veron, P., 1989, *ESO Scientific Report No. 7*
- Vladilo, G. 2004, *A&A*, in press, astro-ph/0403237
- Vladilo, G., Bonifacio, P., Centurion, M., & Molaro, P. 2000, *ApJ*, 543, 24
- Wang, J., Hall, P. B., Ge, J., Li, A., & Schneider, D. P. 2004, *ApJ*, in press, astro-ph/0404151
- Welty, D., Lauroesch, J., Blades, J., Hobbs, L., & York, D. 1997, *ApJ*, 489, 672
- Welty, D. E., Frish, P., Sonneborn, G. & York, D. G. 1999a, *ApJ*, 512, 636

- Welty, D. E., Hobbs, L. M., Lauroesch, J. T., Morton, D. C., Spitzer, L., & York, D. G. 1999b, *ApJS*, 124, 465
- Welty, D., Lauroesch, J., Blades, J., Hobbs, L., & York, D. 2001, *ApJ*, 554, L75
- Wills, B. J. 1978, in *Pittsburgh Conf. on BL Lac Objects*, ed. A. M. Wolfe (Pittsburgh : Univ. Pittsburgh), 235
- Wolfe, A. M., Lanzetta, K. M., Foltz, C. B., & Chaffee, F. H. 1995, *ApJ*, 454, 698
- York, D. G. et al. 2000, *AJ*, 120, 1579
- York, D. G., & the SDSS Collaboration 2001, *BAAS*, 198, 78.05
- York, D. G. et al. 2005a, in preparation
- York, D. G. et al. 2005b, in preparation

Fig. 1.— Spectrum of Q0738+313 obtained with the MMT blue channel spectrograph.

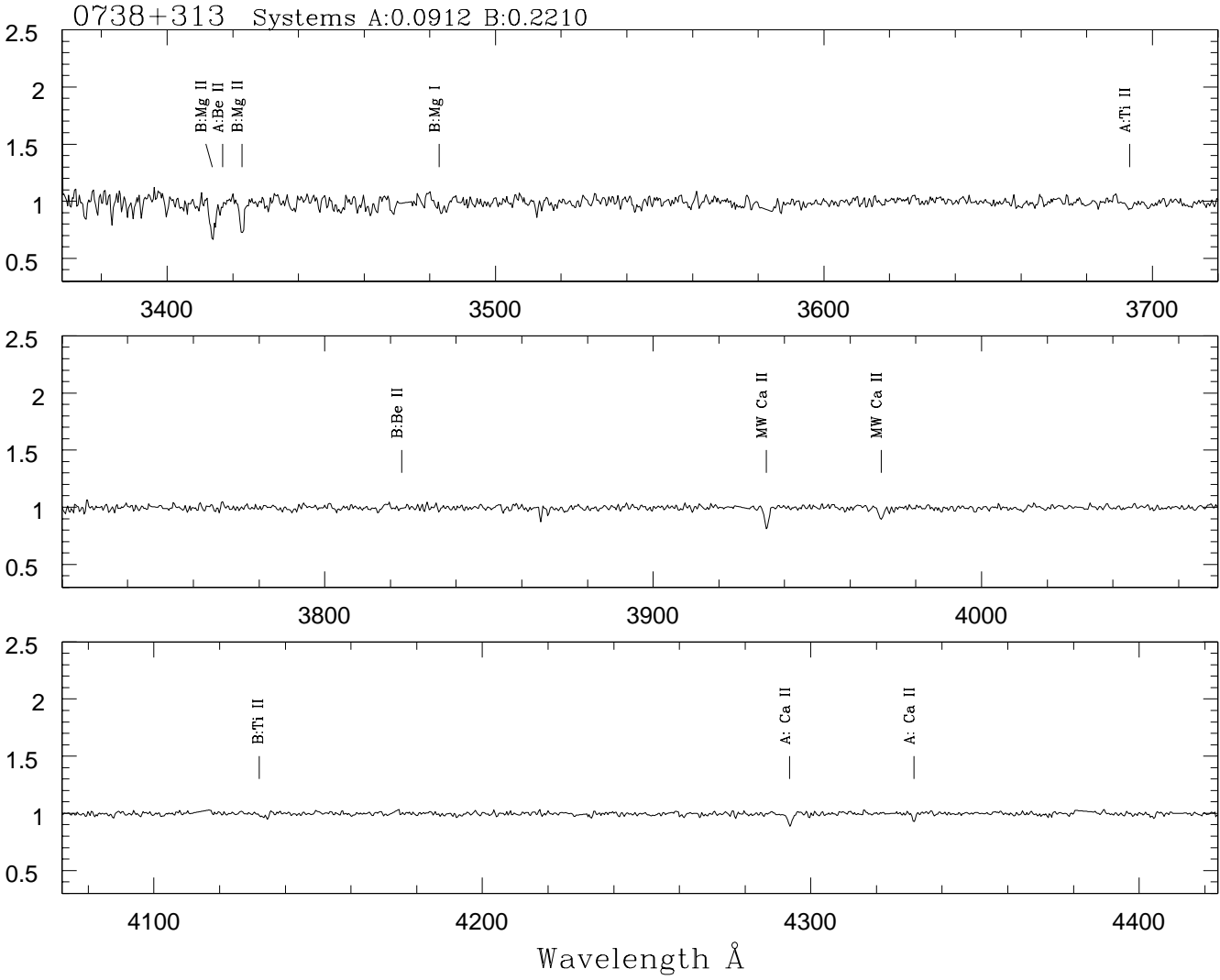


Fig. 2.— Spectrum of Q0827+243 obtained with the MMT blue channel spectrograph.

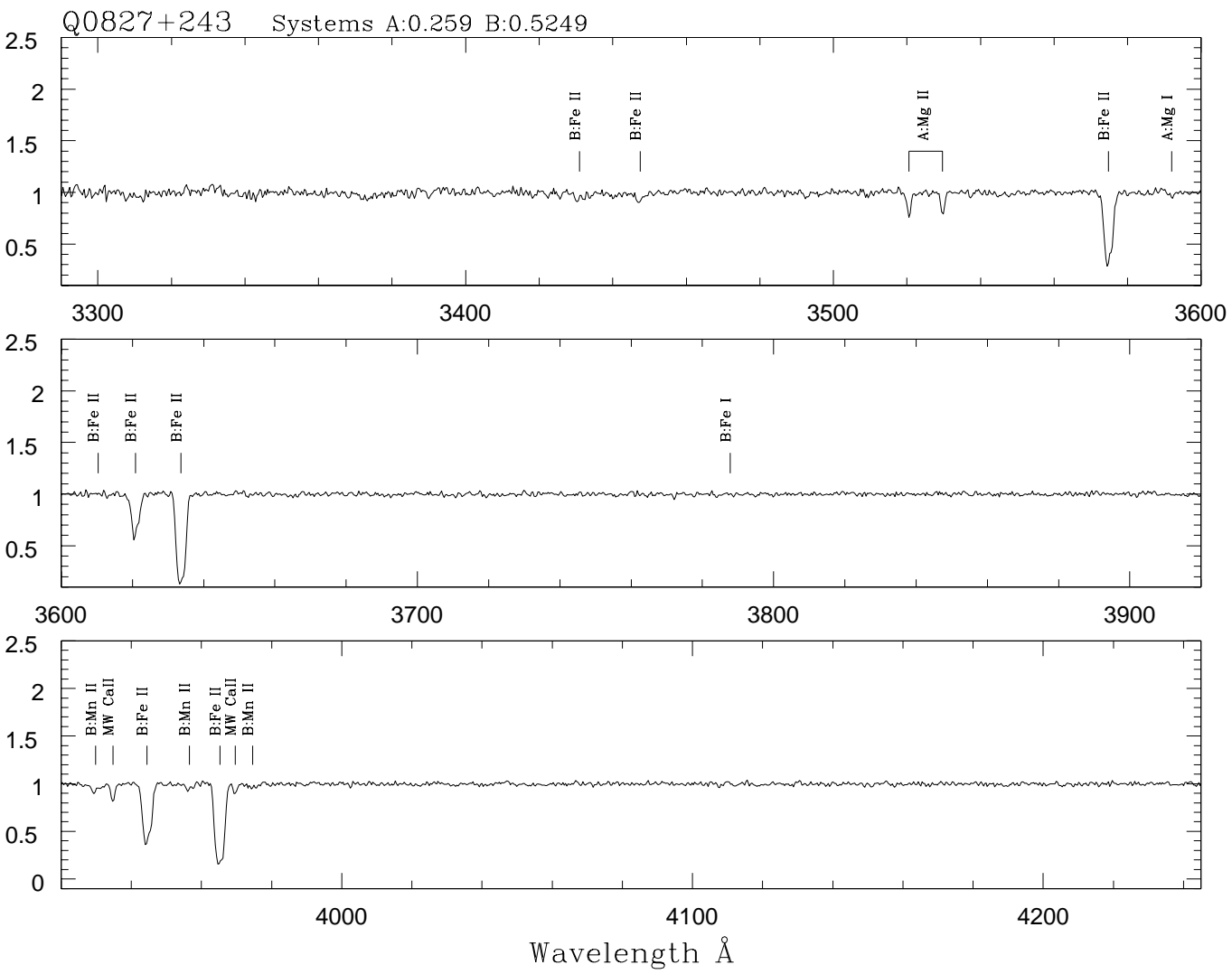
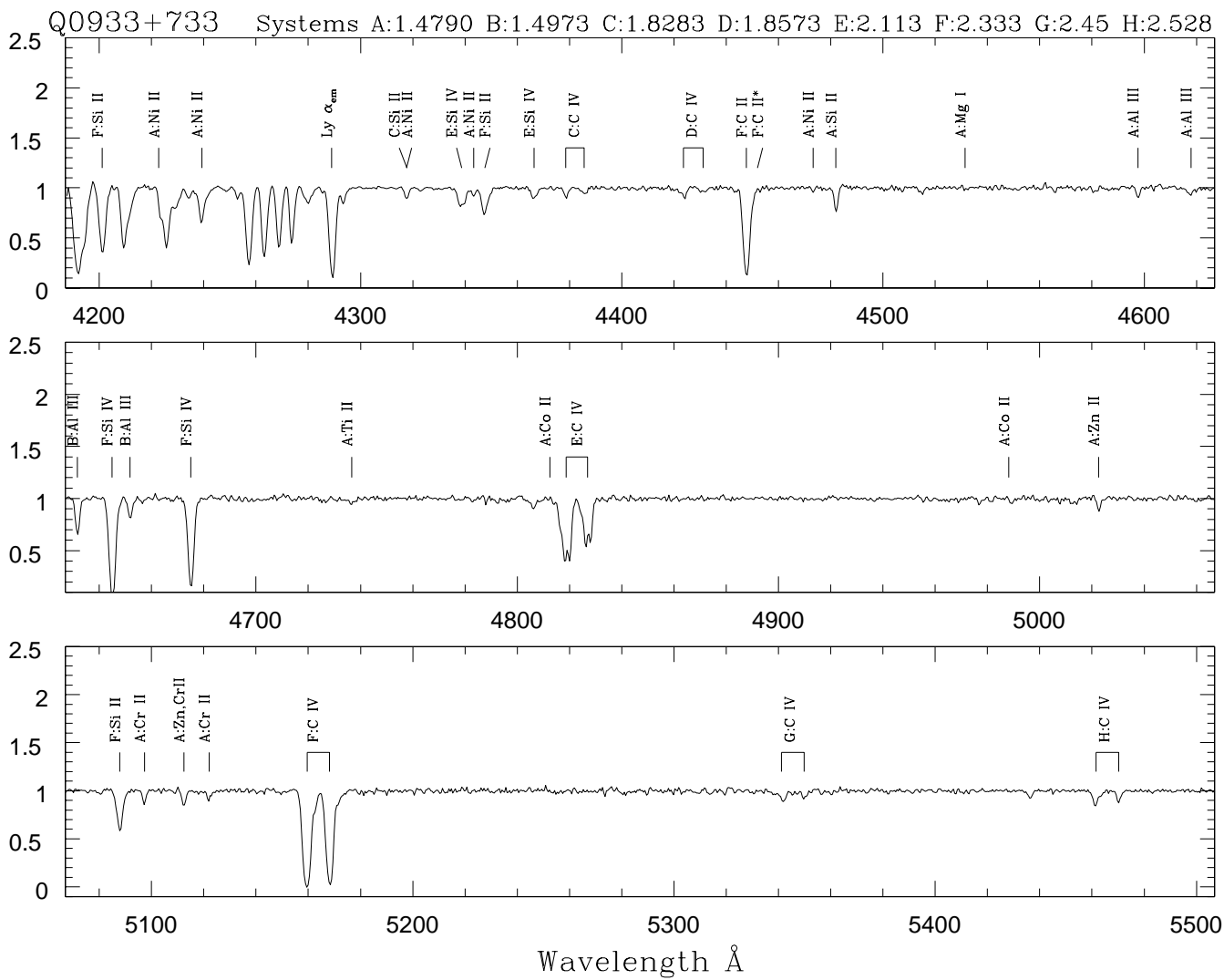


Fig. 3.— Spectrum of Q0933+733 obtained with the MMT blue channel spectrograph.



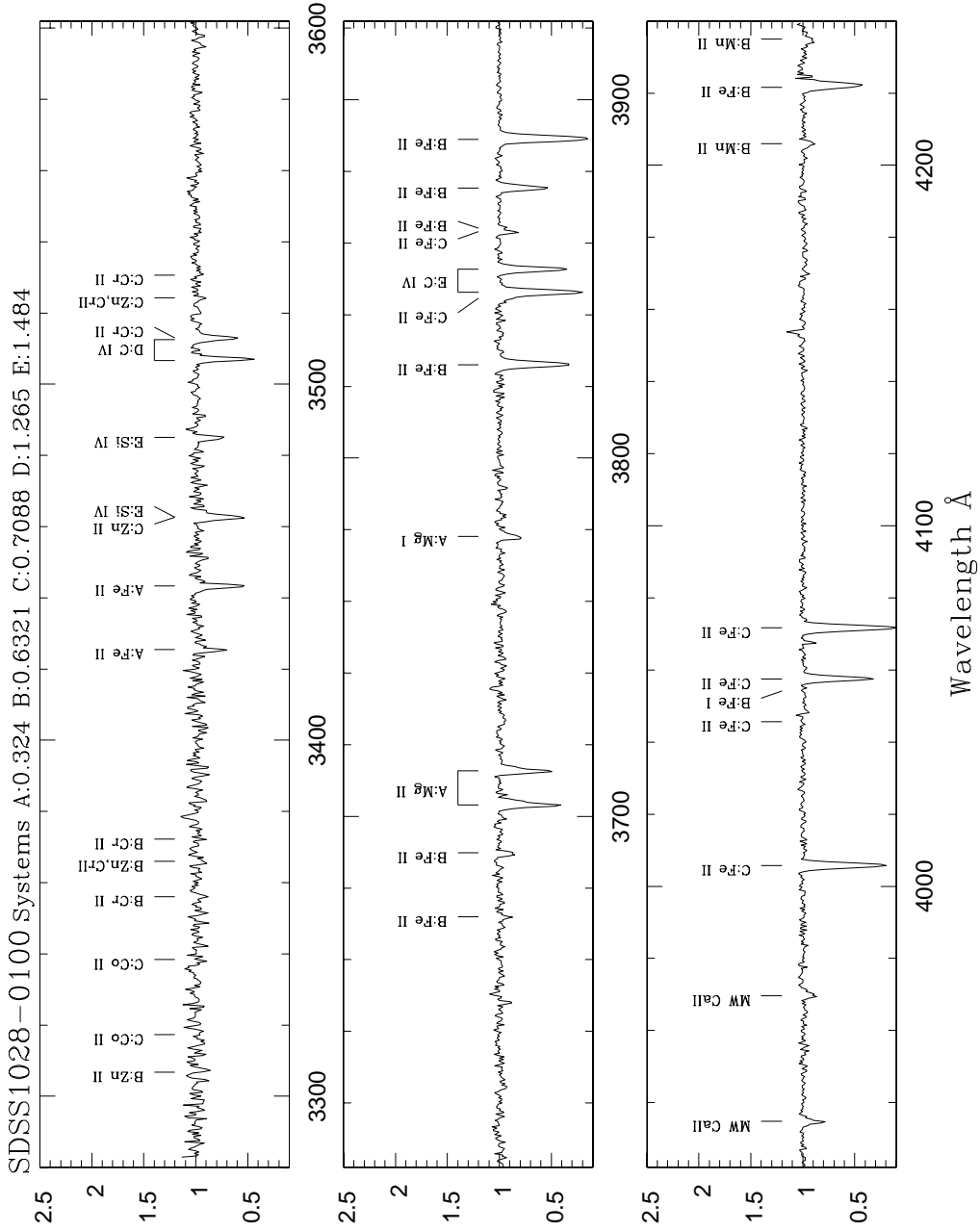


Fig. 4.— Spectrum of SDSSJ1028-0100 obtained with the MMT blue channel spectrograph.

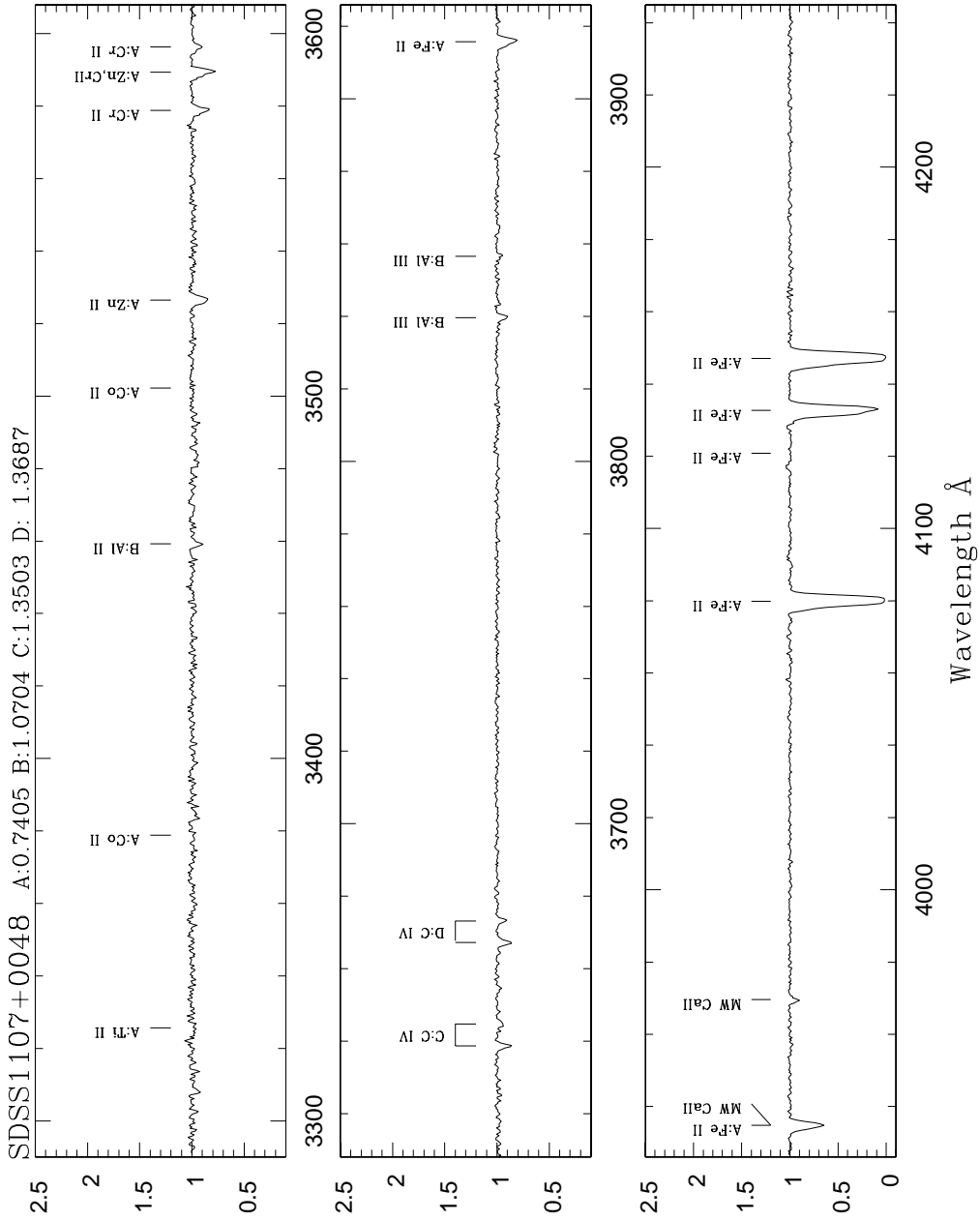
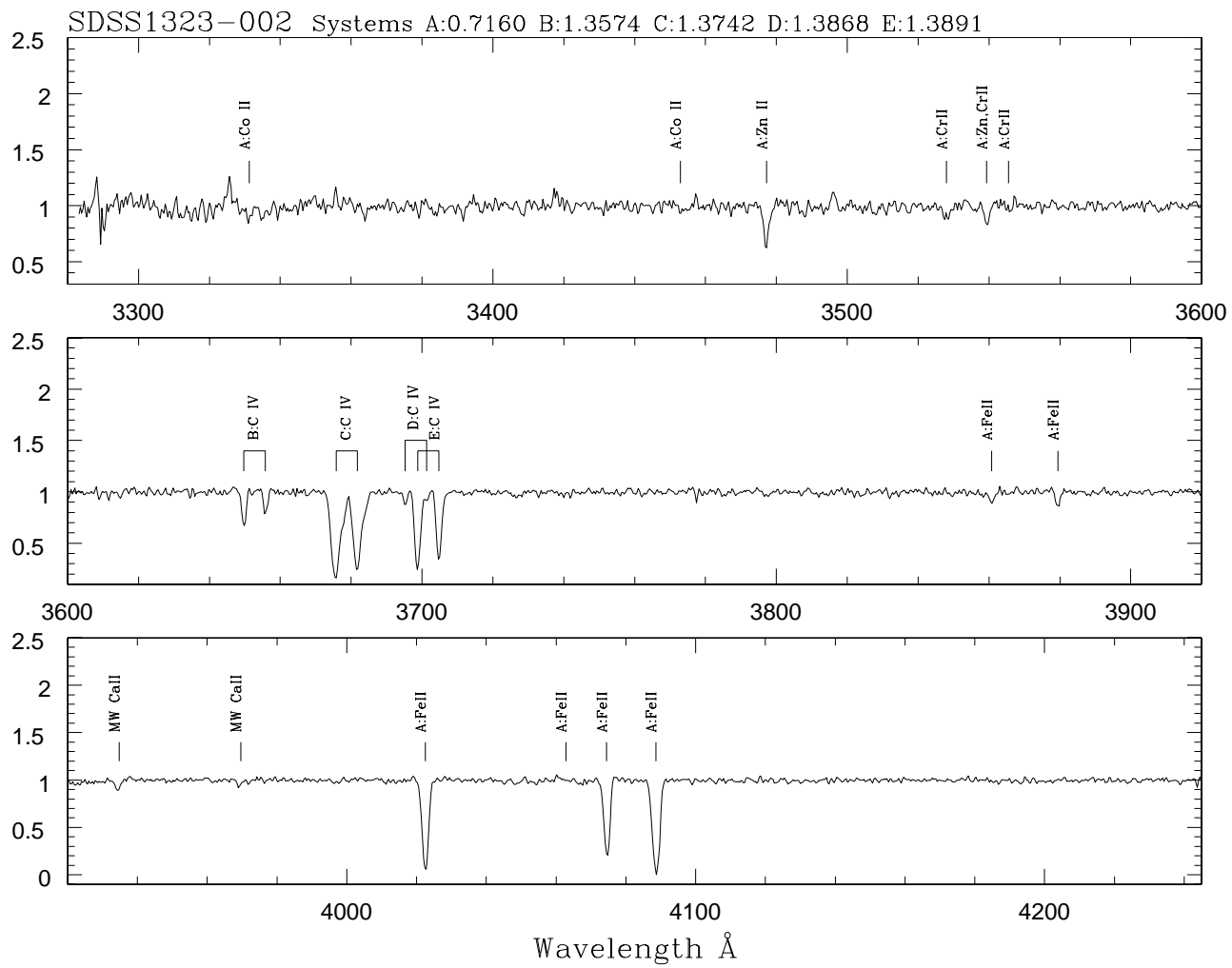


Fig. 5.— Spectrum of SDSSJ1107+0048 obtained with the MMT blue channel spectrograph.

Fig. 6.— Spectrum of SDSSJ1323-0021 obtained with the MMT blue channel spectrograph.



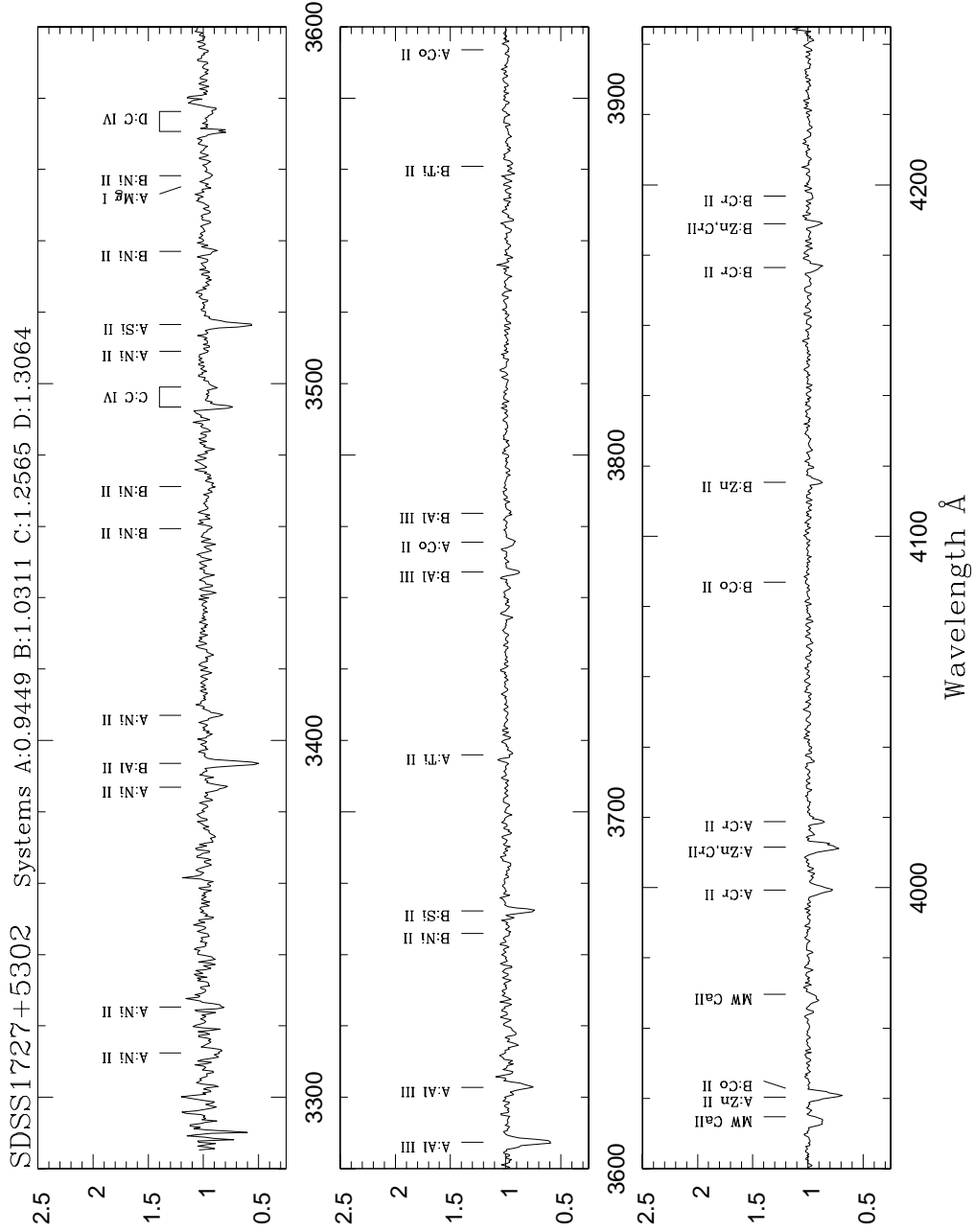


Fig. 7.— Spectrum of SDSSJ1727+5302 obtained with the MMT blue channel spectrograph.

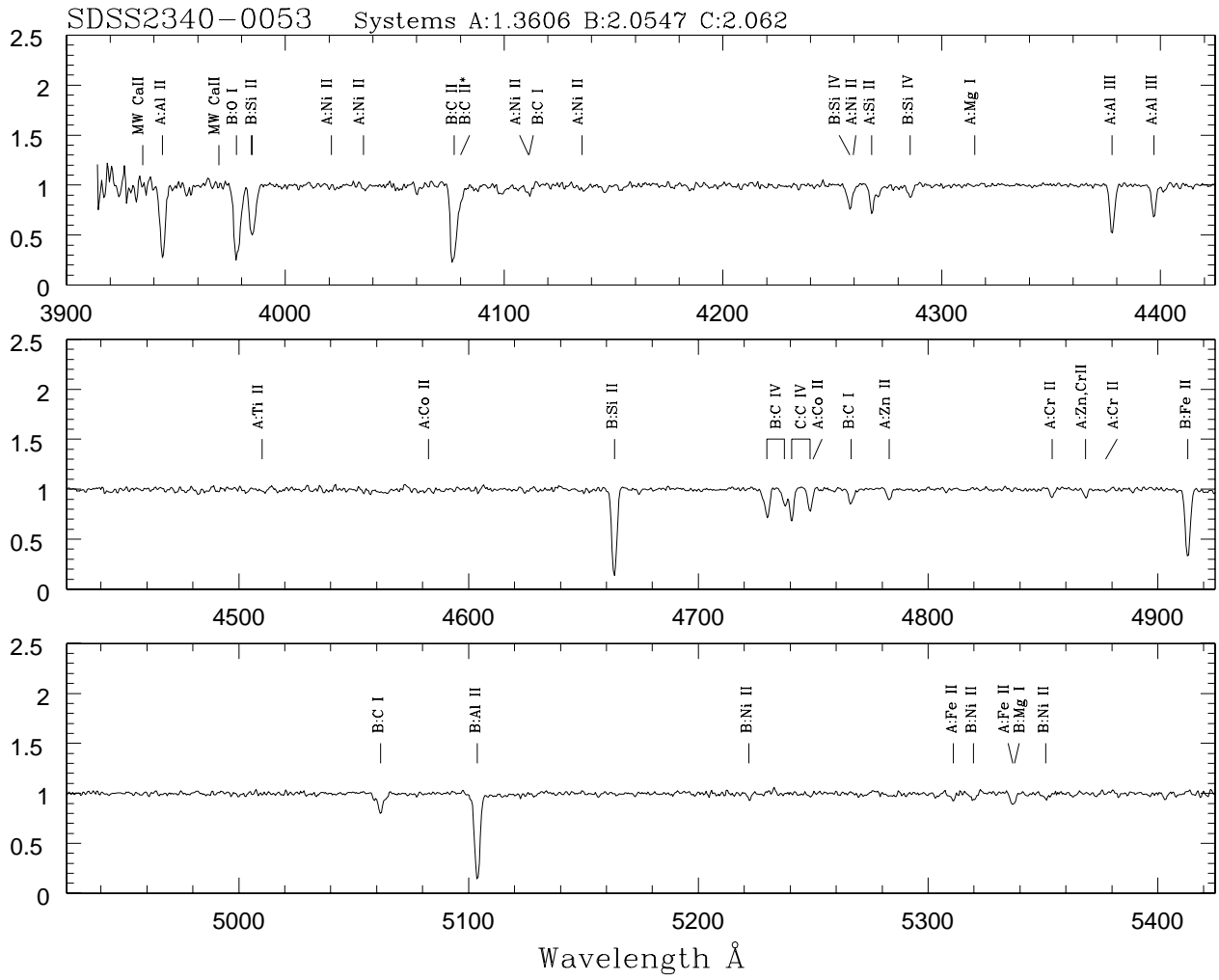


Fig. 8.— Spectrum of SDSSJ2340-0053 obtained with the MMT blue channel spectrograph.

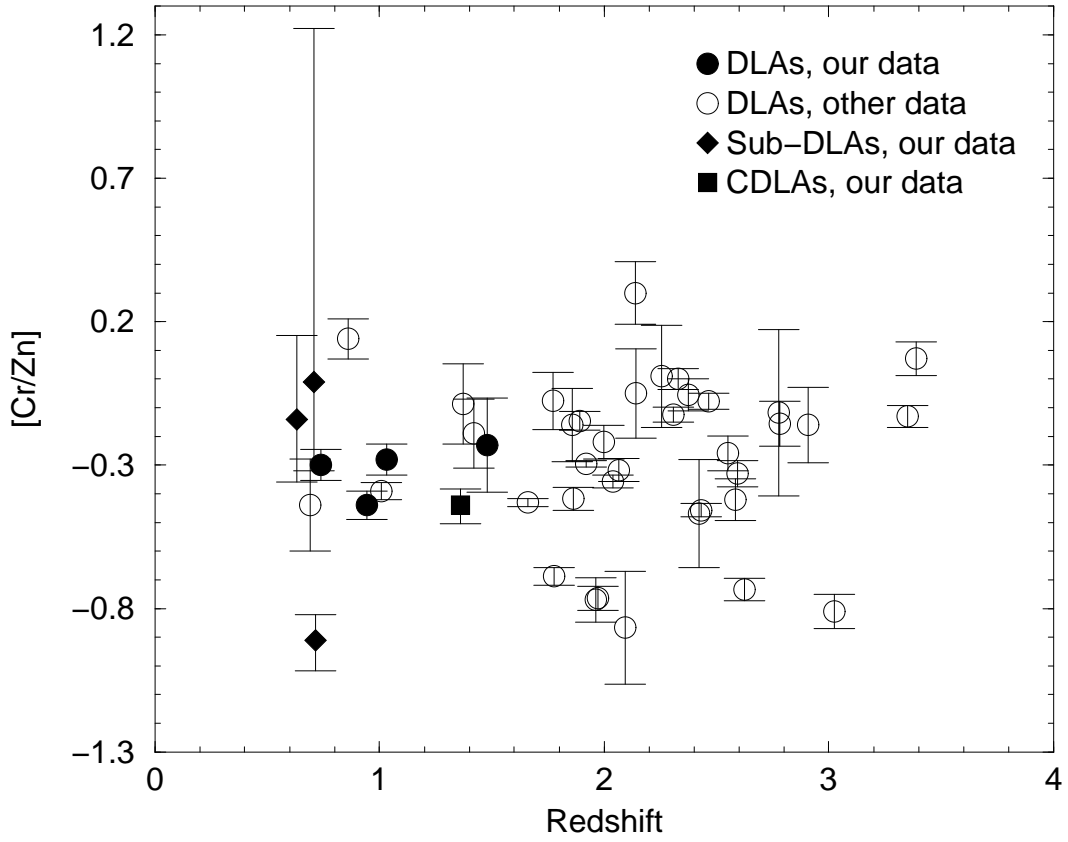


Fig. 9.— $[\text{Cr}/\text{Zn}]$ vs. redshift for DLAs from our MMT survey and other data from the literature. Also shown are values for CDLAs and sub-DLAs from our data.

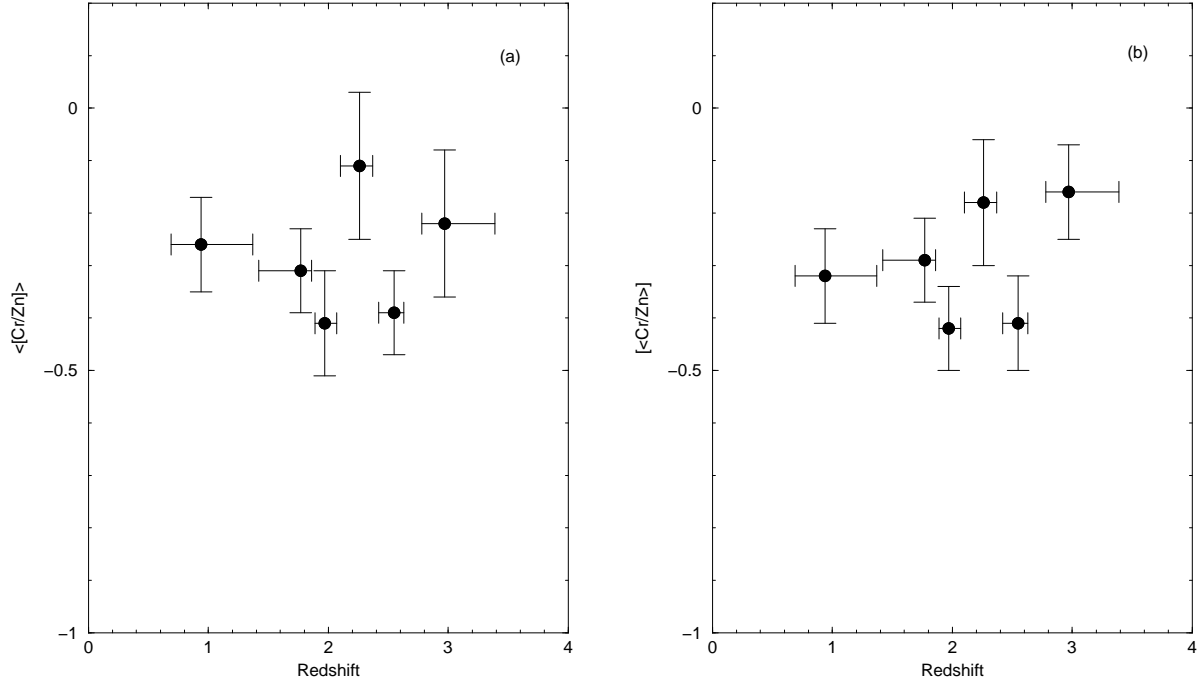


Fig. 10.— a (Left panel): Binned unweighted mean of logarithmic abundance of Cr relative to Zn $\langle [Cr/Zn] \rangle$ vs. redshift for DLAs from our MMT survey and other data from the literature. b (Right panel): Binned logarithm of the N_{ZnII} -weighted mean abundance of Cr relative to Zn $[Cr/Zn]$ vs. redshift for DLAs from our MMT survey and other data from the literature. The zero level in both panels denotes the solar level.

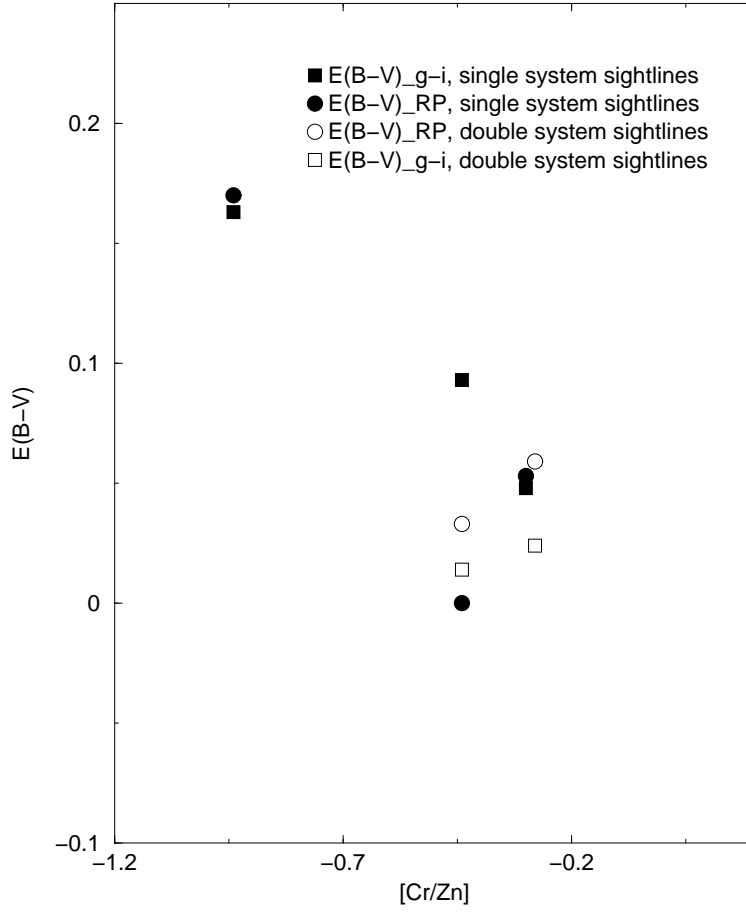


Fig. 11.— Reddening $E(B-V)_{RP}$ or $E(B-V)_{g-i}$ relative to SDSS composite quasar spectra vs. $[Cr/Zn]$ for the SDSS absorbers from our sample.

Table 1. Targets Observed

QSO	Plate	Fiber	MJD	z_{em}	g	z_{DLA}	Grating l/mm	FWHM Å	Time s	S/N
Q0738+313				0.630 ^a	16.10	0.0912	832	1.10	8300 ^e	15-90
Q0738+313				0.630	16.10	0.2210	832	1.10	8300 ^e	15-90
Q0827+243				0.941 ^b	17.26	0.5249	832	1.10	5400 ^f	15-60
Q0933+733				2.525 ^c	17.30	1.4790	1200	1.33	3600 ^f	50-90
SDSS J102837.01-010027.4	273	286	51957	1.532 ^d	18.24	0.6321	832	1.04	9900 ^f	20-55
SDSS J102837.01-010027.4	273	286	51957	1.532 ^d	18.24	0.7088	832	1.04	9900 ^f	20-55
SDSS J110729.03+004811.1	278	378	51900	1.392 ^d	17.66	0.7405	832	1.04	5400 ^f	10-50
SDSS J132323.78-002155.2	297	267	51959	1.390 ^d	18.49	0.7160	832	1.10	13500 ^f	25-55
SDSS J172739.03+530229.1	359	42	51821	1.444 ^d	18.45	0.9449	832	1.10	14400 ^f	35-70
SDSS J172739.03+530229.1	359	42	51821	1.444 ^d	18.45	1.0311	832	1.10	14400 ^f	35-70
SDSS J234023.66-005327.0	385	204	51877	2.085 ^d	17.84	1.3606	1200	1.50	18900 ^e	50-90

^aVeron-Cetty & Veron (1989)

^bUlrich & Owen (1977)

^cSteidel & Sargent (1992)

^d<http://skyserver2.fnal.org>

^eObserved in October, 2002

^fObserved in March, 2003

Table 2. Other data^a

QSO	z_{abs}	FeII	FeII	FeII	FeII	FeII	MnII	MnII	MnII	MgII	MgII	MgI	CaII	CaII
		2344	2374	2382	2586	2600	2576	2594	2606	2796	2803	2853	3933	3969
0738 ^b	0.22					<0.6				0.52	0.50	< 0.2		
0827 ^c	0.53					1.90				2.90	2.20			
0933 ^d	1.48	0.53	0.78	0.57	0.43	0.76				0.95	1.15	< 0.3		
		0.05	0.07	0.05	0.06	0.08				0.08	0.09			
1028 ^{e,f}	0.63	0.88		0.94	0.80	1.13	< 0.12	< 0.12	< 0.12	1.61	1.36	0.48	0.52	0.39
		0.15		0.13	0.18	0.12				0.11	0.11	0.11	0.11	0.11
1028 ^{e,f}	0.71	0.79	0.61	1.09	0.98	0.87			0.36	1.22	1.08	0.72		
		0.13	0.13	0.19	0.12	0.11			0.08	0.08	0.09	0.11		
1107 ^e	0.74	1.98	1.58	2.18	2.02	2.31	0.42	0.18	0.24	2.86	2.71	0.84	0.41	0.28
		0.03	0.03	0.03	0.03	0.03	0.03	0.03	0.03	0.03	0.03	0.03	0.04	0.04
1323 ^e	0.72	1.68	1.17	1.46	1.43					2.41	2.13	0.95		
		0.17	0.17	0.15	0.11					0.09	0.09	0.07		
1727 ^e	0.95	1.65	1.24	2.01	1.79	2.16	< 0.08	< 0.08	< 0.08	2.75	2.60	0.94	0.65	0.88
		0.08	0.06	0.08	0.08	0.08				0.09	0.09	0.09	0.09	0.20
1727 ^e	1.03	0.56	0.39	0.69	0.54	0.75	< 0.08	< 0.08	< 0.08	1.01	1.00	0.30		
		0.05	0.06	0.06	0.08	0.06				0.07	0.07	0.08		
2340 ^{e,g}	1.36	1.05	0.76	1.15	1.08	1.21	< 0.06	< 0.06	< 0.06	1.55	1.58	0.54	< 0.06	< 0.06
		0.03	0.03	0.03	0.03	0.03				0.03	0.03	0.03		

^aColumns 3 to 15 list the rest equivalent widths in Å, values in odd rows from 5 to 17 are 1 σ errors

^bBoisse et al. (1992)

^cWills 1978 and Ulrich & Owen (1977)

^dSteidel & Sargent, (1992)

^eYork et al. (2000); Stoughton et al. (2002); Aberjazian et al. (2003)

^fPetitjean et al. (1998): Si II(λ 1526): B(0.51), C(0.46); Al II(λ 1670): B(0.55), C(0.64); Al III(λ 1862): B(0.33), Al III(λ 1854): C(0.26)

^gAdditional SDSS data :

Al II (λ 1670) : 0.92 \pm 0.05 ; Si II (λ 1808):0.29 \pm 0.03 ; Al III(λ 1854): 0.55 \pm 0.04 ; Al III(λ 1862):0.31 \pm 0.04

Table 3 Atomic data

Species	$\lambda_{vac}(\text{\AA})$	f	Ref	Species	$\lambda_{vac}(\text{\AA})$	f	Ref
O I	1302.1685	4.800e-2	a	Cr II	2056.2569	1.050e-1	a,c
Si II	1304.3702	8.630e-2	a	Cr II	2062.2361	7.800e-2	a,e
Si IV	1393.7602	5.130e-1	a	Zn II	2062.6604	2.560e-1	a,e
Si IV	1402.7729	2.540e-1	a	Cr II	2066.161	5.150e-2	e
C IV	1548.204	1.899e-1	a	Fe II	2249.8768	1.820e-3	f
C IV	1550.781	9.475e-2	a	Fe II	2260.7805	2.440e-3	f
Fe II	1608.4511	5.770e-2	a	Al I	2263.4644	8.920e-2	a
Al II	1670.7874	1.740e-0	a	Fe II	2344.2139	1.140e-1	a,g
Ni II	1703.4119	5.999e-3	a	Fe II	2367.5905	2.160e-5	a
Ni II	1709.6042	3.240e-2	a	Fe II	2374.4612	3.130e-2	a,g
Ni II	1741.549	4.270e-2	a	Fe II	2382.7652	3.200e-1	a
Ni II	1751.910	2.270e-2	a	Fe I	2484.0211	0.621e-0	a
Ni II	1804.473	3.800e-3	b	Mn II	2576.877	3.610e-1	a
Si II	1808.0129	2.080e-3	a,c	Fe II	2586.6500	6.910e-2	a
Mg I	1827.9351	2.420e-2	a	Mn II	2594.499	2.800e-1	a
Al III	1854.7164	5.590e-1	a	Fe II	2600.1729	2.390e-1	a
Al III	1862.7895	2.780e-1	a	Mn II	2606.462	1.980e-1	a
Ti II	1910.6123	1.040e-1	a,d	Mg II	2796.3543	6.155e-1	a
Ti II	1910.9538	9.800e-2	a,d	Mg II	2803.5315	3.058e-1	a
Co II	1941.2852	3.403e-2	a	Mg I	2852.9631	1.830e-0	a
Co II	2012.1660	3.680e-2	a	Be II	3131.3292	3.321e-1	a
Zn II	2026.1370	4.890e-1	a,e	Ti II	3384.7304	3.580e-1	a
Cr II	2026.269	1.300e-3	a,e	Ca II	3934.7750	6.267e-1	a
Mg I	2026.4768	1.130e-1	a	Ca II	3969.5901	3.116e-1	a

References: **a:** Morton, (2003); **b:** Welty et al. (1999); **c:** Bergeson & Lawler (1993a); **d:** Wiese, Fedchak & Lawler (1996); **e:** Bergeson & Lawler (1993b); **f:** Bergeson, Mullman & Lawler (1994) **g:** Bergeson et al. (1996)

Table 4 Equivalent Widths

QSO	z_{abs}	Species	λ_{rest} Å	Δz_{abs}^a	W_{rest} Å	QSO	z_{abs}	Species	λ_{rest} Å	Δz_{abs}^a	W_{rest} Å
0738 A	0.0912	Be II	3131		< 0.1	1028 C	0.7088	Fe II	2249	-14.4	0.08±0.01
		Ti II	3384	-5.0	0.13±0.02			Fe II	2260	-12.5	0.11±0.01
		Ca II	3934	5.8	0.16±0.02			Fe II	2344	5.3	0.78±0.03
		Ca II	3969	-0.8	0.08±0.01			Fe II	2367		<0.13
0738 B	0.2210	Mg II	2796	-7.6	0.61±0.04			Fe II	2374	-0.5	0.44±0.01
		Mg II	2803	-7.3	0.38±0.02			Fe II	2382	7.5	1.05±0.02
		Mg I	2853	14.9	0.24±0.04			Fe I	2484		<0.02
		Be II	3131		<0.03			Mn II	2576	4.6	0.11±0.01
0827 B	0.5249	Ti II	3384		<0.04			Fe II	2586	13.7	0.70±0.02
		Fe II	2249	3.1	0.13±0.01			Mn II	2594	4.4	0.12±0.03
		Fe II	2260	-4.2	0.14±0.01			Co II	1941		<0.06
		Fe II	2344	-5.9	1.11±0.01			Co II	2012		<0.06
		Fe II	2367		<0.03	Zn/Mg ^{b,d}	2026		<0.48		
		Fe II	2374	-2.9	0.67±0.02	Cr II ^d	2056		<0.38		
		Fe II	2382	4.0	1.69±0.02	Zn/Cr ^c	2062		0.05±0.02		
		Fe I	2484		<0.02	Cr II	2066	45.9	0.07±0.02		
		Mn II	2576	0.7	0.20±0.01	Fe II	2249		<0.91		
		Fe II	2586	-0.1	1.19±0.01	Fe II ^d	2260	3.8	0.13±0.01		
		Mn II	2594	0.4	0.10±0.01	Fe II	2344	-3.3	0.79±0.01		
		0933 A	1.4790	Fe II	2600	4.9	1.79±0.02	Fe II	2367		< 0.03
Mn II	2606			-4.2	0.10±0.02	Fe II	2374	0.5	0.60±0.01		
Ni II	1703				<1.06	Fe II	2382	-1.1	0.96±0.01		
Ni II	1709				<1.40	Ti II	1910		<0.02		
Ni II	1741			18.6	0.08±0.01	Co II	1941		<0.02		
Ni II	1751			15.2	0.06±0.01	Co II	2012		<0.02		
Ni II	1804			-3.4	0.02±0.01	Zn/Mg ^b	2026		0.20±0.01		
Si II	1808			-2.3	0.16±0.01	Cr II	2056	-4.3	0.19±0.01		
Mg I	1827				<0.01	Zn/Cr ^c	2062		0.25±0.01		
Al III	1854			-12.8	0.06±0.01	Cr II	2066	13.0	0.12±0.01		
Al III ^d	1862			-1.2	0.08±0.01	Fe II	2249	-2.0	0.26±0.01		
Ti II	1910			-25.6	0.07±0.01	Fe II ^d	2260	-2.7	0.43±0.01		
1028 B	0.6321	Co II	1941		<0.02	Fe II	2344	-3.1	1.95±0.01		
		Co II	2012		<0.02	Fe II	2367		< 0.02		
		Zn/Mg ^b	2026		0.08±0.01	Fe II	2374	0.4	1.56±0.01		
		Cr II	2056	-7.3	0.08±0.01	Fe II	2382	-4.1	2.15±0.01		
		Zn/Cr ^c	2062		0.11±0.01	Co II	1941		<0.04		
		Cr II ^d	2066	5.0	0.06±0.01	Co II	2012		<0.04		
		Zn/Mg ^b	2026		0.08±0.02	Zn/Mg ^b	2026		0.38±0.02		
		Cr II	2056	-8.2	0.09±0.02	Cr II ^d	2056	-16.1	0.18±0.02		
		Zn/Cr ^c	2062		0.09±0.02	Zn/Cr ^c	2062		0.16±0.02		
		Cr II	2066		<0.06	Cr II	2066		<0.04		

Equivalent Widths (cont'd.)

QSO	z_{abs}	Species	λ_{rest} Å	Δz_{abs}^a	W_{rest} Å	QSO	z_{abs}	Species	λ_{rest} Å	Δz_{abs}^a	W_{rest} Å
1727 A	0.9449	Fe II	2249	-10.1	0.11±0.02	2340 A	1.3606	Al III	1854	7.2	0.09±0.01
		Fe II	2260	6.6	0.13±0.01			Al III	1862	16.0	0.04±0.01
		Fe II	2344	5.6	1.26±0.01			Ti II	1910		<0.02
		Fe II	2367		< 0.02			Co II	1941		<0.02
		Fe II	2374	10.1	0.95±0.01			Co II	2012		<0.01
		Fe II	2382	4.0	1.47±0.01			Zn/Mg ^b	2026		0.12±0.01
		Ni II	1703	-32.4	0.20±0.04			Cr II	2056	4.9	0.12±0.01
		Ni II	1709	24.3	0.18±0.02			Zn/Cr ^c	2062		0.08±0.01
		Ni II	1741	-22.4	0.28±0.03			Cr II	2066	7.3	0.04±0.01
		Ni II	1751	-12.1	0.14±0.02			Al II	1670	-11.2	0.89±0.03
		Ni II	1804	-30.8	0.02±0.01			Ni II	1703		< 0.02
		Si II	1808	7.8	0.45±0.02			Ni II	1709	40.4	0.05±0.01
		Mg I	1827		<0.04			Ni II	1741	10.3	0.12±0.01
		Al III	1854	9.9	0.42±0.02			Ni II	1751	8.6	0.10±0.01
		Al III	1862	-9.3	0.26±0.02			Ni II	1804		< 0.29
		Ti II	1910	15.5	0.06±0.01			Si II ^d	1808	3.05	0.29±0.01
		Co II ^d	1941	-6.9	0.08±0.01			Mg I	1827		< 0.02
		Co II	2012		<0.03			Al III	1854	-17.6	0.52±0.01
		Zn/Mg ^b	2026		0.32±0.01			Al III	1862	2.3	0.38±0.01
		Cr II	2056	21.1	0.34±0.02			Ti II	1910		<0.02
Zn/Cr ^c	2062		0.33±0.02	Co II	1941		<0.2				
Cr II	2066	19.0	0.13±0.01	Co II	2012		<0.20				
1727 B	1.0311	Al II	1670	4.6	0.41±0.02	Zn/Mg ^b	2026		0.10±0.01		
		Ni II	1703		0.05±0.02	Cr II	2056	0.5	0.07±0.01		
		Ni II	1709	-32.9	0.10±0.03	Zn/Cr ^c	2062		0.07±0.01		
		Ni II	1741	-8.7	0.08±0.01	Cr II	2066		<0.02		
		Ni II	1751	16.1	0.08±0.02	Fe II	2249	-22.9	0.07±0.02		
		Si II	1808	1.9	0.19±0.01	Fe II ^d	2260	7.3	0.13±0.01		

a : In units of 10^{-5}

b : Zn II (2026) is blended with Mg I (2026)

c : Zn II (2062) is blended with Cr II (2062)

d : Blend

Table 5 Column Densities

QSO	z_{abs}	Species	$\log N$ cm^{-2}	b_{eff} km s^{-1}	QSO	z_{abs}	Species	$\log N$ cm^{-2}	b_{eff} km s^{-1}
0738 A	0.0912	H I ^a	$21.18_{0.06}^{0.05}$		1028 C	0.7088	H I ^c	$20.01_{0.17}^{0.12}$	
		Be II	<12.70	10.0			Mg I ^b	$13.13_{0.17}^{0.19}$	30.0
		Ca II	$12.31_{0.03}^{0.03}$	42.3 ± 6.9			Al II ^b	14.19	30.0
		Ti II	$12.53_{0.06}^{0.14}$	42.3			Al III ^b	13.34	30.0
0738 B	0.2210	H I ^a	$20.90_{0.09}^{0.07}$		1107 A	0.7405	Si II ^b	14.81	30.0
		Be II	<12.04	10.0			Cr II	$13.23_{0.11}^{0.09}$	30.0
		Mg I	$12.00_{0.12}^{0.09}$	37.8			Mn II ^b	$13.33_{0.19}^{0.17}$	30.0
		Mg II	$>13.30_{0.03}^{0.03}$	37.8 ± 6.3			Fe II	$14.94_{0.03}^{0.03}$	30.0 ± 0.7
		Ti II	<12.11	10.0			Co II	<13.74	10.0
0827 B	0.5249	H I ^a	$20.30_{0.05}^{0.04}$		1323 A	0.7160	Zn II	$12.22_{1.23}^{0.29}$	30.0
		Mn II	$12.83_{0.34}^{0.19}$	$38.2, 28.7$			H I ^c	$20.98_{0.17}^{0.12}$	
		Fe I	<11.72	10.0			Mg I	$12.73_{0.82}^{0.27}$	80.7 ± 20.4
		Fe II	$14.59_{0.02}^{0.02}$	38.2 ± 1.9			Ti II	<12.82	10.0
		Fe II	$14.23_{0.03}^{0.03}$	28.7 ± 1.1			Cr II	$13.75_{0.03}^{0.03}$	80.7 ± 20.4
0933 A	1.4790	H I ^a	$21.62_{0.09}^{0.08}$		1727 A	0.9449	Mn II ^b	$13.34_{0.07}^{0.04}$	80.7
		Mg I	<12.75	28.6			Fe II	$15.52_{0.06}^{0.06}$	89.5 ± 3.5
		Al III	$12.67_{0.05}^{0.04}$	31.3 ± 14.5			Co II	<13.18	10.0
		Si II	$15.52_{0.03}^{0.03}$	28.6 ± 7.5			Zn II	$13.03_{0.05}^{0.05}$	80.7 ± 20.4
		Ti II	$12.85_{0.09}^{0.21}$	28.6			H I ^c	$20.21_{0.18}^{0.21}$	
		Cr II	$13.46_{0.09}^{0.08}$	28.6			Mg I ^b	$13.15_{0.08}^{0.07}$	47.0
		Fe II ^b	14.34	28.6			Cr II	$13.33_{0.10}^{0.08}$	47.0
		Co II	<13.30	10.0			Fe II	$15.11_{0.03}^{0.03}$	47.0 ± 1.0
		Ni II	$13.91_{0.01}^{0.01}$	37.2 ± 18.1			Co II	<13.60	10.0
		Zn II	$12.67_{0.16}^{0.12}$	28.6			Zn II	$13.25_{0.04}^{0.04}$	47.0
1028 B	0.6321	H I ^c	$19.90_{0.17}^{0.12}$		1727 A	0.9449	H I ^d	$21.16_{0.16}^{0.11}$	
		Mg I ^b	$12.80_{0.28}^{0.20}$	26.7			Mg I	$12.90_{0.50}^{0.23}$	69.2 ± 4.2
		Al II ^b	14.06	26.7			Al III	$13.49_{0.02}^{0.02}$	69.3 ± 4.9
		Al III ^b	13.85	26.7			Si II	$15.94_{0.02}^{0.02}$	61.4 ± 4.9
		Si II ^b	15.28	26.7			Ti II	$12.90_{0.12}^{0.09}$	37.2 ± 44.6
		Cr II	$13.34_{0.15}^{0.11}$	26.7			Cr II	$13.85_{0.02}^{0.02}$	69.2 ± 4.2
		Mn II	$12.83_{0.33}^{0.19}$	64.6 ± 18.9			Fe II ^b	$15.38_{0.15}^{0.13}$	69.2 ± 4.2
		Fe I	< 11.86	10.0			Co II	<13.29	10.0
		Fe II	$15.07_{0.05}^{0.04}$	26.7 ± 6.7			Ni II	$14.27_{0.08}^{0.07}$	73.1 ± 23.9
		Zn II	$12.46_{0.27}^{0.16}$	26.7			Zn II	$13.27_{0.05}^{0.04}$	69.2 ± 4.2

Column Densities(cont'd)

QSO	z_{abs}	Species	$\log N$ cm^{-2}	b_{eff} km s^{-1}	QSO	z_{abs}	Species	$\log N$ cm^{-2}	b_{eff} km s^{-1}
1727	1.0311	H I ^d	$21.41_{0.15}^{0.11}$		2340	1.3606	Mg I	$12.83_{0.15}^{0.11}$	33.7 ± 8.2
B		Mg I ^b	$12.45_{0.02}^{0.01}$	32.4 ± 8.3	A		Al I	< 12.49	10.0
		Al II	$13.15_{0.02}^{0.02}$	44.4 ± 3.6			Al II	$13.53_{0.02}^{0.02}$	84.3 ± 4.9
		Al III	$12.75_{0.06}^{0.05}$	33.2 ± 17.7			Al III	$13.63_{0.01}^{0.01}$	65.1 ± 2.4
		Si II	$15.60_{0.03}^{0.03}$	39.9 ± 9.0			Si II	$15.70_{0.02}^{0.02}$	49.8 ± 6.5
		Ti II	< 12.92	10.0			Ti II	< 12.71	10.0
		Cr II	$13.39_{0.03}^{0.03}$	32.4 ± 8.3			Cr II	$13.20_{0.04}^{0.04}$	33.7 ± 8.2
		Fe II ^b	14.54	32.4			Fe II	$14.94_{0.15}^{0.11}$	53.2 ± 43.5
		Co II	< 13.00	10.0			Co II	< 13.30	10.0
		Ni II	$13.91_{0.08}^{0.07}$	39.4 ± 23.0			Ni II	< 13.74	10.0
		Zn II	$12.65_{0.05}^{0.04}$	32.4 ± 8.3			Zn II	$12.62_{0.05}^{0.04}$	33.7 ± 8.2

^a:Rao & Turnshek, (2000)

^b:Calculated from equivalent width in Table 2

^c:HST GO Project No. 9382, P.I. Rao, S.

^d:Turnshek et al. (2004)

Table 6. Relative Abundances

QSO	z_{abs}	[Cr/Zn]	[Fe/Zn]	[Ni/Zn]	[Si/Zn]	[Ti/Zn]	[Co/Zn]	[Mn/Zn]	[Al/Zn]	[Si/Fe]
0827	0.53
0933	1.48	-0.2	-1.2 ^a	-0.4	-0.1	-0.1	<0.4	1.1 ^a
1028	0.63	> 0.3	>-0.4	...	>-0.2 ^a	>-0.6	>-0.2 ^a	0.1 ^a
1028	0.71	>-0.5	>-0.6	...	>-0.8 ^a	>-0.2 ^a	>-0.3 ^a	-0.2 ^a
1107	0.74	-0.3	-0.4	<-0.5	< -0.1	-0.6 ^a
1323	0.72	-0.9	-1.0	<0.1
1727	0.95	-0.4	-0.7 ^a	-0.6	-0.2	-0.7	< -0.3	0.5 ^a
1727	1.03	-0.3	-1.0 ^a	-0.3	0.0	<0.0	<0.1	...	-1.2	1.0 ^a
2340	1.36	-0.4	-0.5	<-0.5	0.2	<-0.2	<0.4	...	-0.6	0.7
Mean ^b	< 1.5	-0.4	-0.8	-0.4	0.0	-0.4	...	-0.6	-0.9	0.5
Mean ^c	> 2.5	-0.4	-0.5	-0.4	0.1	-0.9	0.4
GWC ^{d,e}		-1.0	-1.2	-1.2	-0.2	-1.0	-0.7	-0.8	-0.9	1.0
GCC ^{d,f}		-1.7	-1.8	-1.8	-0.9	-2.4	-1.7	-1.1	-2.0	0.9
HC ^{d,g}		-0.5	-0.5	-0.5	-0.2	-0.6	...	-0.1	...	+0.3

^aValues based on data in Table 2, assuming b value to be same as that of Zn

^bNote that the limits on relative abundances have been excluded while calculating the mean values

^cAverage values from Prochaska et al. (2003a)

^dWelty et al. (1997,1999a,1999b,2001), York et al. (2005b)

^eGalactic warm clouds

^fGalactic cold clouds

^gGalactic halo clouds

Table 7 Reddening Characteristics for SDSS Quasars in Our Sample

QSO	z_{em}	α_{RP}	$E(B - V)_{RP}$	$\Delta(g - i)$	$E(B - V)_{g-i}$	Visual Notes
SDSSJ1028-0100	1.531 ^a	-0.02	...	very blue
SDSSJ1107+0048	1.392	+0.30	0.05	0.14	0.05	very blue
SDSSJ1323-0021	1.390	+0.06	0.17	0.47	0.16	somewhat red, but no 2200 Å dip
SDSSJ1727+5302	1.444	+0.35	0.09	0.13	0.04	blue
SDSSJ2340-0053	2.085	-1.00	0.00	0.39	0.09	somewhat red, but no 2200 Å dip

^aReliable $E(B - V)_{RP}$ is not available for this object.

Table 8 Rough Constraints on H I column densities and abundances of Zn and Ti

QSO	z_{abs}	N_{HI}	[Zn/H]	[Ti/H]
Q0738+313	0.091	1.5×10^{21a}		-1.6
Q0738+313	0.221	7.9×10^{20a}		<-1.7
Q0933+733	1.479	4.2×10^{21a}	-1.6	-1.7
SDSSJ1107+0048	0.741	9.7×10^{20b} 2.3×10^{21c}	-0.6	< -1.1
SDSSJ1323-0021	0.716	1.6×10^{20b} 7.5×10^{21c}	0.4	
SDSSJ1727+5302	0.945	1.5×10^{21d}	-0.5	-1.2
SDSSJ1727+5302	1.031	2.6×10^{21d}	-1.4	<-1.4
SDSSJ2340-0053	1.361	4.3×10^{21c}	-1.6	

^aHST data: Rao & Turnshek, (2000)

^bHST GO Project No. 9382, P.I. Rao, S.; see Table 5 for error estimates

^cEstimates based on reddening

^dHST data: Turnshek et al. (2004)